Developmental Cell

Hippo Reprograms the Transcriptional Response to Ras Signaling

Highlights

- Hippo pathway determines Ras signaling output of differentiation or proliferation

- Ras signaling mediates cell fate decisions as well as proliferation during development

- Scallopped controls expression of Ras effectors Pointed and Capicua

- Hippo signaling and Capicua repress a gene subset required for excessive proliferation

Authors

Justine Pascual, Jelle Jacobs,
Leticia Sansores-Garcia, ...,
Stein Aerts, Georg Halder,
Fisun Hamaratoglu

Correspondence

stein.aerts@kuleuven.be (S.A.),
georg.halder@vib.be (G.H.),
fisun.hamaratoglu@unil.ch (F.H.)

In Brief

How is the cellular response to Ras activation—differentiation versus proliferation—determined? Pascual et al. show that the Hippo pathway helps decide by controlling expression of Ras effector genes, including the repressor Capicua. Capicua acts with Hippo signaling to repress and restrict the expression of a gene subset to prevent hyperproliferation.

CrossMark

CellPress

Article

Hippo Reprograms the Transcriptional Response to Ras Signaling

Justine Pascual,[1,7] Jelle Jacobs,[2,3,7] Leticia Sansores-Garcia,[2] Malini Natarajan,[4,6] Julia Zeitlinger,[4,5] Stein Aerts,[3,*] Georg Halder,[2,*] and Fisun Hamaratoglu[1,8,*]

[1]Center for Integrative Genomics, University of Lausanne, 1015 Lausanne, Switzerland
[2]VIB Center for Cancer Biology and KU Leuven Department of Oncology, University of Leuven, 3000 Leuven, Belgium
[3]Laboratory of Computational Biology, Center for Human Genetics, and VIB-KU Leuven Center for Brain & Disease Research, University of Leuven, 3000 Leuven, Belgium
[4]Stowers Institute for Medical Research, Kansas City, MO 64110, USA
[5]Department of Pathology and Laboratory Medicine, University of Kansas Medical Center, Kansas City, KS 66160, USA
[6]Present address: Department of Molecular Biology, Cell Biology and Biochemistry, Brown University, Providence, RI 02912, USA
[7]These authors contributed equally
[8]Lead Contact
*Correspondence: stein.aerts@kuleuven.be (S.A.), georg.halder@vib.be (G.H.), fisun.hamaratoglu@unil.ch (F.H.)
http://dx.doi.org/10.1016/j.devcel.2017.08.013

SUMMARY

Hyperactivating mutations in Ras signaling are hallmarks of carcinomas. Ras signaling mediates cell fate decisions as well as proliferation during development. It is not known what dictates whether Ras signaling drives differentiation versus proliferation. Here we show that the Hippo pathway is critical for this decision. Loss of Hippo switches Ras activation from promoting cellular differentiation to aggressive cellular proliferation. Transcriptome analysis combined with genetic tests show that this excessive proliferation depends on the synergistic induction of Ras target genes. Using ChIP-nexus, we find that Hippo signaling keeps Ras targets in check by directly regulating the expression of two key downstream transcription factors of Ras signaling: the ETS-domain transcription factor Pointed and the repressor Capicua. Our results highlight how independent signaling pathways can impinge on each other at the level of transcription factors, thereby providing a safety mechanism to keep proliferation in check under normal developmental conditions.

INTRODUCTION

The development of cancer usually requires the accumulation of multiple genetic aberrations, with most tumors having two to six driver mutations (Kandoth et al., 2013; Tomasetti et al., 2015). Some of the most frequent driver mutations occur in components of the epidermal growth factor receptor (EGFR)-Ras-Raf-MAPK pathway, hereafter referred to as the Ras pathway. EGFR is mutated or amplified in nearly one-fifth of all cancers tested, and mutations in the downstream effectors KRAS and BRAF are found in 22.4% and 18.7% of all cancer samples tested, respectively, as tabulated in the COSMIC (Catalog of So-

matic Mutations in Cancer) database (Forbes et al., 2015). These cancer-associated mutations cause hyperactivation of the Ras pathway and provide a major contribution to transformation of a normal cell into a cancer cell (Lemmon and Schlessinger, 2010; Burgess, 2008; Vakiani and Solit, 2011). However, hyperactivation of Ras signaling by itself is not sufficient to cause cellular transformation. Thus, activating mutations in the Ras pathway cause only a mild excess in proliferation in different animal models, but can lead to aggressive and metastatic tumors in combination with mutations in other genes such as p53, the cell polarity proteins Scribbled and Discs-large, or components of the JNK and Hedgehog (Hh) signaling pathways (Xia and Land, 2007; Pagliarini and Xu, 2003; Wu et al., 2010; Schnidar et al., 2009; Pearson et al., 2011; Brumby and Richardson, 2003; Chabu et al., 2017; Uhlirova and Bohmann, 2006). However, the underlying mechanisms leading to excess proliferation in response to these combinatorial mutations remain largely unknown. Here, we show that mutations in Hippo signaling strongly synergize with activated Ras signaling and dissect out the underlying mechanism of this synergistic interaction using genomics, genetics, and computational approaches. We find that the transcriptional output of Ras signaling is under the tight control of the Hippo pathway. Given that p53, Hh, Scribbled, and Discs-large all modulate Hippo signaling (Colombani et al., 2006; Richardson and Portela, 2017; Kagey et al., 2012), our findings also provide a model for how these molecules synergize with Ras during tumorigenesis.

The Hippo pathway is known for its key role in controlling organ growth and progenitor cell proliferation (Hariharan, 2015; Halder and Johnson, 2011; Pan, 2010; Barry and Camargo, 2013). Named after its founding kinase Hippo (Hpo), the pathway coordinately regulates cell proliferation and cell death. Cells that lack Hippo signaling proliferate faster and are resistant to apoptotic stimuli, a combination that leads to dramatic tissue overgrowths in flies and mice. Notably, loss of Hippo signaling in the mouse liver leads to tumor formation (Zhou et al., 2009; Song et al., 2010; Lee et al., 2010; Lu et al., 2010) and YAP, the transcriptional effector of Hippo signaling, is an established oncogene in the ovary, lung, liver, and breast (Harvey et al., 2013; Zanconato et al., 2016).
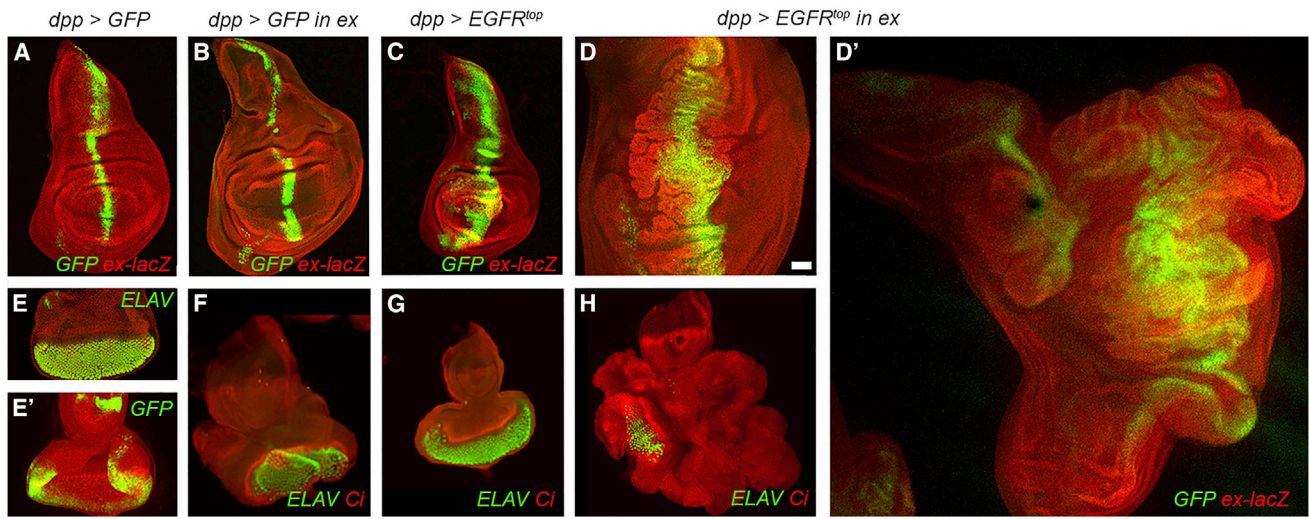
dpp > GFP   *dpp > GFP in ex*   *dpp > EGFR*top   *dpp > EGFR*top *in ex*

Figure 1. Activated EGFR Can Induce Either Differentiation or Proliferation

(A–H) Wing (A–D′) and eye-antennal (E–H) imaginal discs from late third-instar larvae expressing the indicated UAS transgenes with the *dpp-Gal4* driver. (A and E′) The expression pattern of *dpp-Gal4* (green). *ex-lacZ* is shown in red (A–D′), Ci antibody marks the morphogenetic furrow (MF) (red in F–H), and photoreceptor cells are labeled with ELAV antibodies (green in E–H). (B) Homozygous *ex* mutant discs are slightly overgrown and (F) have defects in the movement of the MF in the eye. (C) Expression of activated EGFR (EGFR^{top}) in the *dpp* stripe (green) leads to expansion of this region and (G) induces ectopic photoreceptor differentiation. (D and H) The same construct (EGFR^{top}) induces massive overgrowth in the absence of *ex*. Scale bar in (D), 50 μm (all images are shown on the same scale). Genotypes: (A) and (E): *w; ex^{e1}/+; dpp-Gal4, UAS-GFP^{nls}/+*; (B) and (F): *w; ex^{e1}/ex^{AP50}; dpp-Gal4, UAS-GFP^{nls}/+*; (C) and (G): *w; dpp-Gal4, UAS-GFP^{nls}/UAS-EGFR^{top}*; (D), (D′), and (H): *w; ex^{e1}/ex^{AP50}; dpp-Gal4, UAS-GFP^{nls}/UAS-EGFR^{top}*. See also Figure S1.

The components and mechanisms of Hippo signaling are highly conserved in animals. At the core of the Hippo pathway is a kinase cascade where in *Drosophila* the Hpo kinase (Mst1/2 in mammals) phosphorylates and activates the Warts kinase (Wts; Lats1/2 in mammals). The main substrate of activated Wts/Lats is the transcriptional co-activator Yorkie (Yki; YAP/TAZ in mammals), which is retained in the cytoplasm upon phosphorylation. In the absence of Hippo pathway activity, Yki translocates into the nucleus and binds to the TEAD family transcription factor Scalloped (Sd; TEAD1–4 in mammals) and other transcription factors. By default Sd is a repressor, but the binding of Yki converts Sd into an activator and together they then drive the expression of pro-survival and proliferation genes, such as *cyclin E*, *diap-1*, and *bantam* microRNA (Koontz et al., 2013; Hariharan, 2015). Multiple upstream regulators including the FERM domain proteins Merlin (Mer) and Expanded (Ex), the atypical cadherins Fat and Dachsous, cell polarity, and mechanical forces have been shown to activate the Hpo kinase (Grusche et al., 2010; Piccolo et al., 2014; Legoff et al., 2013; Mao et al., 2013; Karaman and Halder, 2017).

Here, we studied the effects of combining mutations in the Ras and Hippo pathways. Notably, reducing Hippo signaling in cells harboring activating mutations in the Ras pathway caused strongly synergistic overgrowth in *Drosophila* imaginal discs. We find that in such discs, the differentiation program is shut down. We investigated the molecular basis of this synergy using genomics and show that the Hippo pathway acts as a gatekeeper for Ras signaling output by restricting the expression levels of its transcriptional targets. This is achieved via direct transcriptional control of the transcription factors of the Ras

pathway. In *Drosophila*, MAPK regulates gene expression by modulating the protein stability of three transcription factors: the repressor Capicua (Cic) and the ETS-domain proteins Pointed (Pnt) and Yan (Shilo, 2014; Jiménez et al., 2012). We show that Cic and Pnt are direct Yki/Sd targets. Thus, in healthy cells, Hippo signaling acts as a brake that restrains the tumorigenic potential of activating mutations in the Ras pathway. Inactivating mutations in the Hippo pathway, however, unmask this potential and synergistically promote hyperproliferation and tumor development.

RESULTS

Simultaneous Deregulation of Ras and Hippo Signaling Induces Synergistic Overgrowth

To study the effects of combinatorial mutations in the Ras and Hippo pathways, we simultaneously activated Ras signaling and repressed the Hippo pathway in *Drosophila* imaginal discs, simple epithelial structures that are widely used to investigate mechanisms of growth control and tissue patterning. To activate Ras signaling, we expressed constitutively active oncogenic versions of EGFR (EGFR^{top}), Ras (Ras^{V12}), or Raf (Raf^{GOF}) (Queenan et al., 1997; Scholz et al., 1997; Stemerdink and Jacobs, 1997; Brand and Perrimon, 1994). To deregulate Hippo signaling, we used animals that were homozygous for null mutations in the Hippo pathway component *expanded* (*ex*) (Hamaratoglu et al., 2006). Loss of *ex* does not fully abolish Hippo pathway activity, and *ex* mutant wing discs showed mild overgrowth characteristic for hypomorphic Hippo loss-of-function phenotypes (Figures 1A and 1B). Similarly, overexpression of activated EGFR in a central stripe in wing discs using the *dpp-Gal4* driver only caused
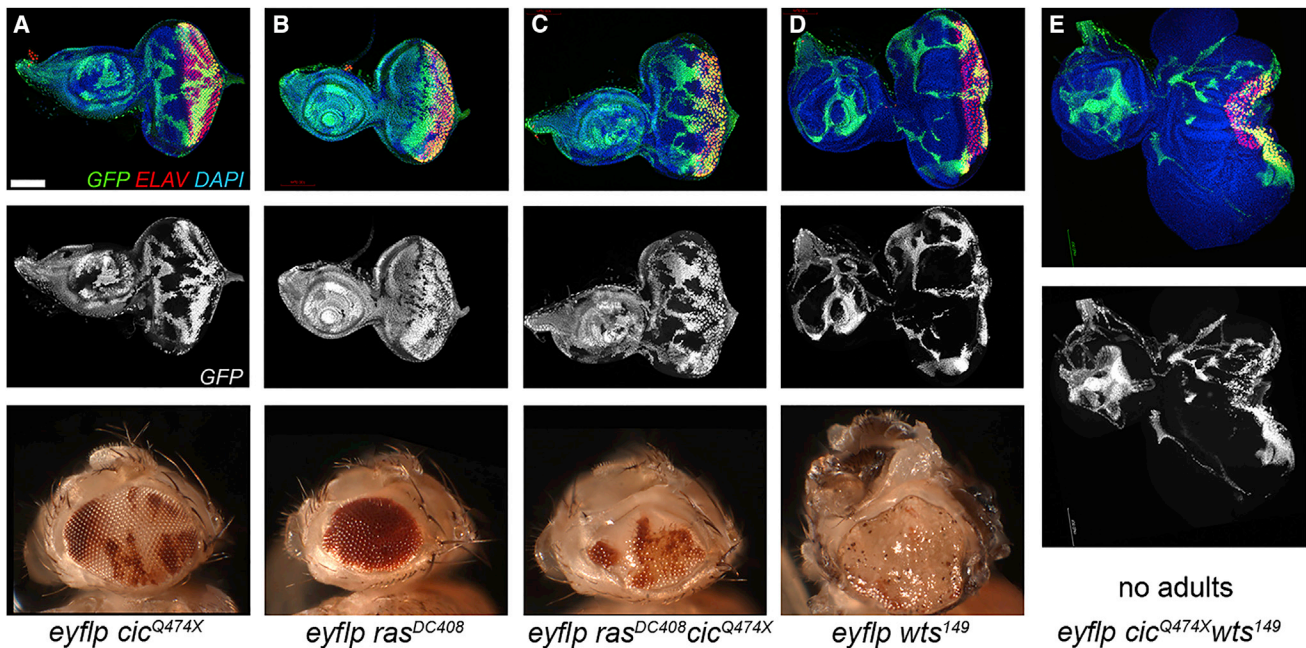
Figure 2. The Synergy between the Two Pathways Is at the Level of Transcriptional Regulation

(A–E) Third-instar eye-antennal imaginal discs (top row) and male fly heads (bottom row) carrying *eyflp* (expressed only in the head) induced clones of indicated genotypes. Mutant clones are marked by the absence of GFP (green in top row, gray in middle row) or lack of mini-w⁺ expression (red in bottom row). (A) cic^{Q474X} mutant cells occupy roughly half the tissue and have no effect on photoreceptor differentiation marked by ELAV (red), (B) ras^{DC408} mutant clones are small in the larval eye and do not contribute to the adult tissue, (C) further deletion of *cic* rescues the proliferation but not the differentiation defects of ras^{DC408} mutant cells, (D) wts^{149} mutant cells overproliferate, and (E) cic^{Q474X} wts^{149} double-mutant cells induce overgrowth and many folds in the tissue. The eye field is very small. All discs are from day-5 larvae and are shown at the same magnification. See Figure S5B for older discs. Scale bar in (A), 100 μm (all images are shown on the same scale).

Genotypes: (A): *y w eyflp/y w; FRT82B ubiGFP^{nls}/FRT82B cic^{Q474X}*; (B): *y w eyflp/y w; FRT82B ubiGFP^{nls}/FRT82B ras^{DC408}*; (C): *y w eyflp/y w; FRT82B ubiGFP^{nls}/FRT82B ras^{DC408} cic^{Q474X}*; (D): *y w eyflp/y w; FRT82B ubiGFP^{nls}/FRT82B wts^{149}*; (E): *y w eyflp/y w; FRT82B ubiGFP^{nls}/FRT82B cic^{Q474X} wts^{149}*.

a widening of the expression domain marked by GFP co-expression (Figure 1C). Strikingly, however, expressing activated EGFR in *ex* mutants caused massive overgrowth of mutant wing discs (Figures 1D and 1D′). Double-mutant larvae pupated up to 2 days later than controls when discs continued to grow, and eventually folded onto themselves. Such cooperative overproliferation in response to EGFR/Ras activation was formerly described in cells that harbor mutations in the Hippo pathway components *fat* (Garoia et al., 2005) and *wts* (Pagliarini and Xu, 2003). Notably, expression of activated Ras or Raf in *ex* mutants caused the same dramatic overgrowth phenotypes (Figure S1A). Furthermore, the enormous overgrowths in the presence of EGFR^top and *ex* mutants was evident in multiple tissues including eye, antenna, wing, leg, and haltere imaginal discs (Figures 1E–1H and not shown). Therefore, activated Ras signaling synergistically interacts with deregulated Hippo signaling to drive tissue overgrowth, and this interaction is independent of the type of imaginal discs.

The Synergy between Ras and Hippo Signaling Occurs via the Downstream Effectors Cic and Yki

We next investigated at which level of the signal transduction cascades the synergy operates. First, we overexpressed EGFR^top together with Yki, the downstream transcriptional co-activator of the Hippo pathway. Again this caused highly synergistic overgrowth phenotypes (Figure S1A), indicating that the

synergy operates at the level of the downstream transcription effector of the Hippo pathway.

To determine the level of interaction in the Ras pathway, we next tested mutations in the Cic transcription factor. Cic is an HMG-domain transcriptional repressor that mediates the effect of Ras on cell proliferation during eye imaginal disc development (Tseng et al., 2007). Cic is a suppressor of cell proliferation in imaginal discs and activated MAPK phosphorylates Cic, causing its degradation. Ras signaling is required for cell proliferation and cell type specification. Thus, cells with a complete loss of Ras signaling, due to mutations in *egfr*, *ras*, or *raf*, do not proliferate and fail to differentiate (Figures 2A and 2B) (Yang and Baker, 2001; 2003). The failure of *ras* mutant cells to proliferate is due to ectopic Cic activity because *ras*, *cic* double-mutant cells proliferate normally (Figure 2C) (Tseng et al., 2007). Despite the strong rescue in cell proliferation, removal of Cic does not rescue the photoreceptor specification defects of *ras* mutant cells. Double-mutant cells contribute to the adult eye, but cannot differentiate into photoreceptor cells (Figure 2C). Therefore, Cic is a major effector of Ras signaling in proliferation control (Tseng et al., 2007).

We then analyzed the interaction between loss of Cic and loss of Hippo signaling. While deletion of *cic* alone increased cell proliferation in eye discs only slightly, if at all (Figure 2A), simultaneous deletion of *cic* together with *wts* enhanced the *wts* mutant phenotype and triggered massive overgrowth
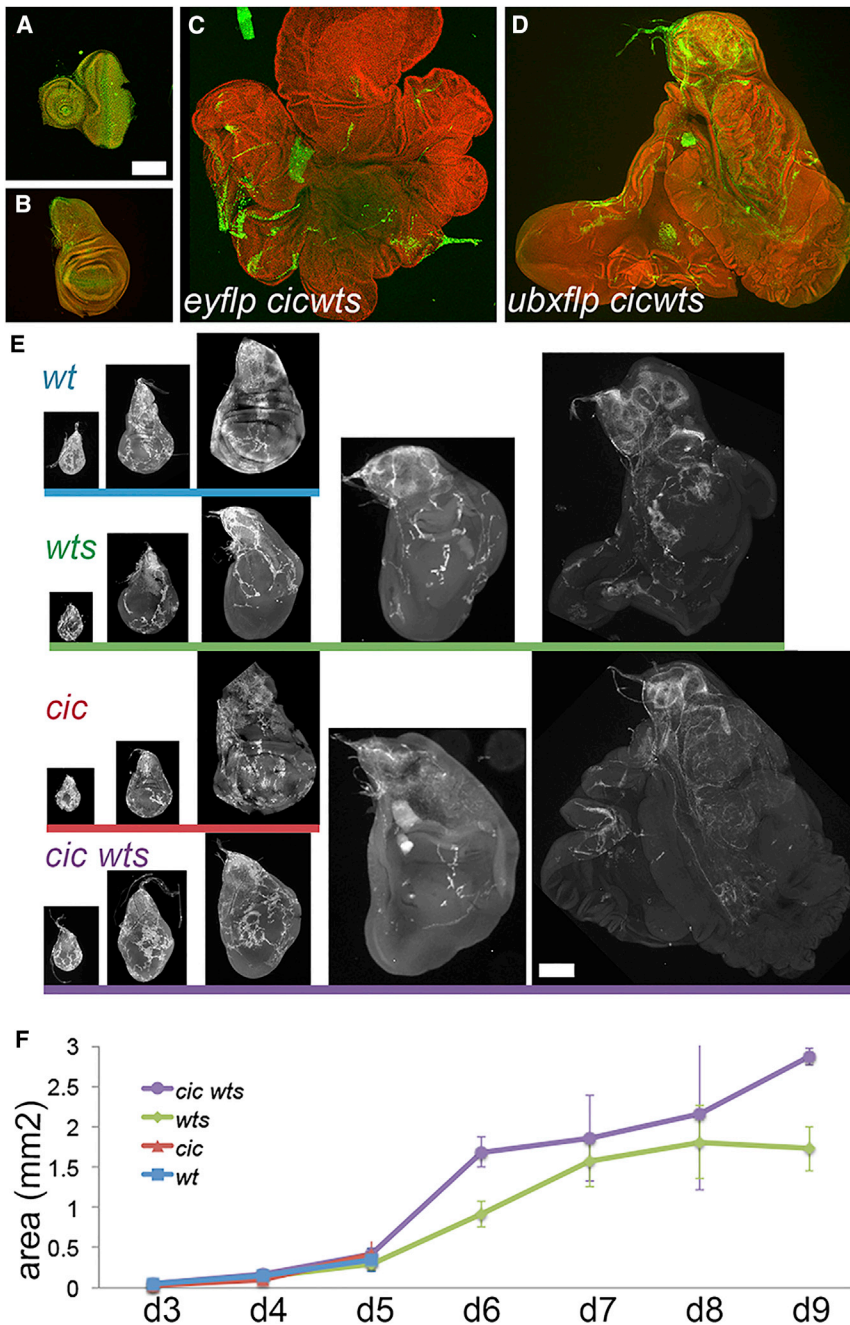
Figure 3. Combined Mutations in *cic* and *wts* Induce Tremendous Overgrowth and Delayed Pupation

(A and B) Control wing and eye discs at the end of larval development.

(C and D) Eye and wing discs with cic^{Q474X} wts^{149} double-mutant cells in a Minute background.

(E) Time-course analysis (days 3, 4, 5, 6, and 9) of wing discs with indicated genotypes. Mutations in *wts* lead to delayed pupation.

(F) *ubx-FLP*, *cic wts* discs can grow up to 10-times bigger than a full-grown wild-type wing disc. The graph shows wing area quantification at different time points (n = 3–5 discs per time point per genotype) and in fact underestimates the size of *cic wts* double-mutant discs, as they form many folds and are on average twice as thick as *wts* discs. The error bars represent SD.

Scale bars in (A) and (E), 200 µm (all images are shown on the same scale). Genotypes: (A) and (B): *y w; FRT82B M(3) ubiGFP^nls/FRT82B cic^{Q474X} wts^{149}*; (C): *y w eyflp/y w; FRT82B M(3) ubiGFP^nls/ FRT82B cic^{Q474X} wts^{149}*; (D): *y ubxflp/y w; FRT82B M(3) ubiGFP^nls/FRT82B cic^{Q474X} wts^{149}*; (E) and (F): *wt*: *y ubxflp/y w; FRT82B M(3) ubiGFP^nls/FRT82B*; *wts*: *y ubxflp/y w; FRT82B M(3) ubiGFP^nls/FRT82B wts^{149}*; *cic*: *y ubxflp/y w; FRT82B M(3) ubiGFP^nls/ FRT82B cic^{Q474X}*; *cic wts*: *y ubxflp/y w; FRT82B M(3) ubiGFP^nls/FRT82B cic^{Q474X} wts^{149}*. See also Figure S4 for *cic* clones in *ex* and *wts* mutant discs.

themselves (Figures 3A–3D). Time-course analysis and quantifications showed that animals with *cic wts* double-mutant wing discs had larval periods extended by about 4 days, similar to animals with *wts* mutant discs. Mutant cells continued to proliferate during this extra time, and *cic wts* double-mutant discs were consistently larger than *wts* discs, reaching up to 10-times the normal disc size (Figures 3E and 3F). Importantly, ectopic Yki also synergized with Cic knockdown in causing tissue expansion (Figures S1B and S1C). Hence, deregulating the Ras and Hippo pathways at the level of their downstream transcription factors produced the same highly synergistic overgrowths. Altogether, these data show that the synergy between the Hippo and Ras pathways is at the level of transcription.

beyond the *wts* phenotype (Figures 2D and 2E). As previously observed, *wts* mutant cells occupied the majority of the tissue and led to overgrown organs (Justice et al., 1995; Xu et al., 1995), and a few animals achieved adulthood (Figure 2D). However, no adults with *cic wts* clones were recovered (Figure 2E).

We then induced clones with the pan-eye and wing disc drivers *ey-FLP* and *ubx-FLP* in combination with the *Minute* technique to produce imaginal discs that were nearly entirely mutant (Figure 3) (Morata and Ripoll, 1975). Eye and wing discs with *cic wts* double-mutant clones had dramatic overgrowth phenotypes that caused the discs to fold onto

Loss of Wts and Cic Synergistically Activates Ras Target Genes

Because the synergy between the Ras and Hippo pathways is at the level of the downstream transcription factors, the two pathways may converge on a set of synergistically regulated target genes that are activated only when both pathways are deregulated. We therefore performed genome-wide expression analyses (RNA sequencing [RNA-seq]) in control, *cic*, and *wts*

single mutant, as well as *cic wts* double-mutant wing discs, to identify synergistically regulated target genes.

Mutations in *wts* cause developmental delay, and we thus produced gene expression profiles by RNA-seq at day 5 in all genotypes and at day 9 in *wts* single-mutant and *cic wts* double-mutant wing discs generated using ubx-FLP and a Minute chromosome (as shown in Figure 3E). We focused on genes with a minimum average expression of 50 counts across all samples, and significant upregulation was defined as a minimum 1.4-fold increase, with less than 1% false discovery rate (log fold change [logFC] > 0.5 and adjusted p-value < 0.01). We found that the expression of 350 genes was significantly upregulated in day-5 *cic wts* double-mutant wing discs compared with discs with wild-type control clones. Importantly, cell polarity was intact in the day-5 *cic wts* discs (see Figure S1D for polarity at day 8), hence the transcriptional changes we see at this stage are not a consequence of polarity loss. We then classified these genes into four different groups, based on day-5 expression levels, using SOTA (self-organizing tree algorithm), an unsupervised clustering method (Herrero et al., 2001; Dopazo and Carazo, 1997). The first and largest group comprised 295 genes (84% of differentially expressed genes) that were upregulated in *wts* single-mutant and *cic wts* double-mutant discs, but not affected in *cic* mutants (Figure 4A). The upregulation of these genes was thus mostly attributed to the *wts* mutation, and we refer to this group as the "Wts cluster." Notably, this cluster contained the known Yki targets *kibra*, *ex*, *wts*, *dm* (also known as *Myc*), and *Ilp8* (also known as *Dilp8*) (Pan, 2007; Boone et al., 2016; Neto-Silva et al., 2010; Park et al., 2016; Ziosi et al., 2010), validating the gene expression data (Figure 4B). *cycE* and *diap1* were also induced in *wts* and *cic wts* mutant discs but their fold increase was below our cutoff with logFC values of 0.37 and 0.35, respectively (Figure 4B). The second and smallest cluster contained only 12 genes, which were upregulated in *cic* and in *cic wts* mutant discs but were not significantly influenced by loss of *wts*, hence we named it the "Cic cluster" (Figure 4C). The genes in this cluster were mostly uncharacterized and non-conserved genes. The third "additive" cluster had 17 genes that were mildly upregulated in *wts* and *cic* single mutants and showed additive upregulation in the double mutant (Figure 4D). These genes are potentially shared target genes of Yki and Cic and included *sdr* (*secreted decoy of InR*), a modulator of insulin signaling (Okamoto et al., 2013), *shifted* (*shf*), a modulator of Hh signaling (Glise et al., 2005; Gorfinkiel et al., 2005), and the ribosomal protein RpL38 (Marygold et al., 2005).

The most interesting fourth cluster had 26 genes that were strongly induced in *cic wts* double mutants but were largely unaffected in *cic* and *wts* single mutants; hence we coined this set the "synergistic cluster" (Figure 4E). In addition to these genes, closer inspection of the *wts* cluster revealed that 28 of the 295 genes were more than 1.3-fold higher in the *cic wts* double mutants compared with *wts* alone, although they were not induced or even downregulated in *cic* clones. These genes were thus also synergistically regulated by Cic and Wts and were reclassified into the synergistic group (Figure 4F).

Surprisingly, the most striking feature of the synergistic genes was a strong signature of Ras pathway target genes. Synergistically upregulated Ras target genes included *argos* (*aos*), which encodes a secreted antagonist of Ras signaling (Golembo et al., 1996; Schweitzer et al., 1995), *sprouty* (*sty*), an intracellular inhibitor of Ras signaling (Casci et al., 1999), and *Nf1*, a negative regulator of Ras activity (Ballester et al., 1990; Martin et al., 1990; Xu et al., 1990; Buchberg et al., 1990). These genes are feedback regulators of Ras signaling in multiple tissues and cell types. Most prominently, the major transcriptional activator of the pathway *pointed* (*pnt*) (Shilo, 2014) was also synergistically induced in the double mutants. These data thus show that Ras signaling output is strongly upregulated in *cic wts* double-mutant cells, much above the levels detected in *cic* or *wts* mutant cells. Therefore, simultaneous loss of *cic* and *wts* resulted in a synergistic hyperactivation of Ras output.

The discovery of 54 genes that were synergistically upregulated in response to concomitant loss of *wts* and *cic* reveals that the synergistic overgrowth phenotype of the double mutant is not a trivial consequence of simultaneous deregulation of two unconnected growth control pathways. Rather, the existence of this synergistic gene set shows that activation of one or the other pathway is not sufficient to upregulate their expression and thus that Cic and Wts act as dominant inhibitors on their expression. The discovery of this synergistically deregulated gene set then prompted two questions. First, what are the transcription factors that regulate the synergistically regulated genes? Second, how does the deregulation of the Hippo pathway induce their expression?

iRegulon Identifies Three Key Transcription Factors that Mediate the Synergy

To understand the mechanisms that regulate the transcription of the synergistic genes and to elucidate how Ras target genes were hyperinduced in double-mutant cells, we searched for transcription factor binding sites that were enriched near the genes of the four gene clusters using iRegulon, a sequence-based motif discovery tool (Janky et al., 2014). iRegulon reverse engineers a gene regulatory network from the expression data by identifying enriched motifs for transcription factors in a given set of genes (Janky et al., 2014). We focused our search on the introns and 5-kb upstream region of each gene. Reassuringly, one of the top motifs (normalized enrichment score [NES] of 4.3, see STAR Methods) in the Wts cluster belonged to the Sd transcription factor, and high-confidence Sd binding sites were detected in 123 of 295 genes in this cluster and in all known direct Sd target genes (Atkins et al., 2016). The very top motif, however, belonged to the AP-1 transcription factors (NES = 4.76), found enriched near 154 genes, indicating the involvement of JNK signaling. Notably, the AP-1 transcription factors, Atf3 and Pdp1, are themselves part of the Wts cluster, suggesting that JNK activation is a downstream effect of Yki activity consistent with the recent literature (Ma et al., 2015). The genes with predicted AP-1 binding sites are induced at similar levels in *wts* and *cic wts* mutant discs (Figure S2A).

Surprisingly, the Cic cluster was not enriched for Cic binding sites, as only one gene, CG32354, had a Cic motif. However, iRegulon analysis on the synergistically induced genes (Figure S2B) identified the Cic binding motif as the top hit with very high confidence (NES = 6.3), followed by Stat92E (NES = 4.3) and Pnt (NES = 3.4) motifs (Figure 5A). Indeed, the previously identified Cic target genes *pnt* and *aos* (Roch et al., 2002; Jin et al., 2015) were in this synergistic cluster. Therefore, we
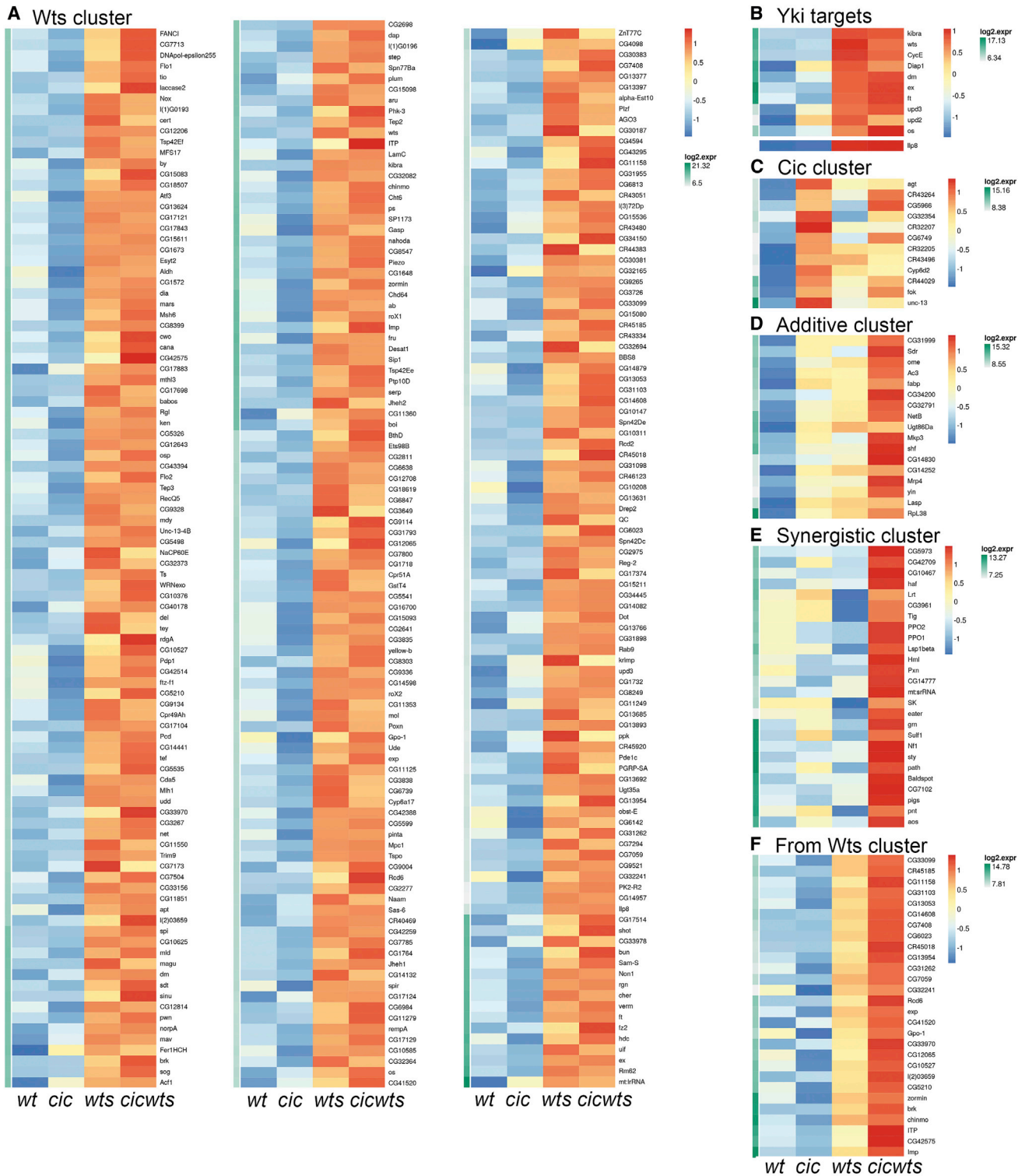
Figure 4. RNA Sequencing Reveals Synergistically Regulated Genes
(A–F) SOTA found four clusters among the 350 upregulated genes in day-5 *cic wts* discs compared with the control discs. Row normalized heatmaps of (A) Wts cluster, (B) known Yki target genes from the Wts cluster. Dilp8 is shown separately as it is most upregulated (28-fold in *wts* discs) and disrupts the visualization of the data when grouped with the other genes. (C) Cic cluster, (D) additive cluster, (E) synergistic cluster, and (F) 28 genes from the Wts cluster that are further upregulated in *cic wts* discs (1.3-fold or more). Green bars represent average expression levels.

Figure 5. Pnt and STAT Are Predicted Key Regulators of the Synergistic Genes and Are Required for the Synergistic Overgrowth

(A) iRegulon predicts that three factors, Cic, Pnt, and Stat92E, regulate the synergistically induced genes. The heatmaps of these 46 synergistic genes are shown in Figure S2B. Eight genes whose expression did not stay elevated at day-9 cic wts discs were removed from the group as they are unlikely to drive the synergistic pheno-type.

(B) iRegulon analysis on Cic target genes returns the same network as shown in (A). The heatmaps of these 19 direct Cic target genes are shown in Figure S2C.

(C) Heatmap showing the expression levels of JAK-STAT ligands Upds and the transcription factors of Ras signaling, Pnt and Cic, in different genotypes and time points.

(D–J) Seven-day-old wing (top) and eye-antennal (bottom) imaginal discs of indicated genotypes. UAS-driven GFP (green) marks the expression domain of the dpp-Gal4 driver. Nuclei are shown in red marked by DAPI (D–G) or ex-lacZ expression (I and J). (H) Quantification of the wing disc areas with our synergistic combination (activated EGFR expression in ex mutant background [dark gray]) and upon additional knockdown of pnt (light gray) at different time points. We measured at least six discs per genotype. For $dpp > EGFR^{top}$ in ex: day 5, n = 11; day 6, n = 10; day 7, n = 9. For $dpp > EGFR^{top} + pnt-RNAi$ in ex: day 5, n = 6; day 6, n = 10; day 7, n = 9. The error bars represent SD.

Scale bar in (F), 100 μm (all images are shown on the same scale). Genotypes: (D) and (E): y w; $FRT40A ex^{AP50}/FRT40A ex^{e1}$; $UAS-EGFR^{top}/dpp$-Gal4, UAS-GFP; (F) and (G): y w; $FRT40A ex^{BQ} UAS-SOCS-36E/FRT40A ex^{e1}$; $UAS-EGFR^{top}/dpp$-Gal4, UAS-GFP; (I) and (J): y w; $FRT40A ex^{AP50}/FRT40A ex^{e1}$; $UAS-EGFR^{top}/dpp$-Gal4, UAS-GFP, UAS-pnt-RNAi (UAS-pnt-RNAi is BL31936). See also Figure S2.

embarked to determine whether other synergistically regulated genes are also direct Cic targets.

Cic Directly Regulates Synergistically Induced Genes

We defined Cic target genes genome-wide using ChIP-nexus (chromatin immunoprecipitation experiments with nucleotide resolution through exonuclease, unique barcode, and single liga-tion), a robust ChIP-exo protocol that allows high-resolution mapping of binding sites (He et al., 2015). We used the Cic signal in cic wts mutant discs as background. Combining the ChIP-nexus signal with motif enrichment to determine high-confi-dence Cic peaks, we identified over 100 regions bound by Cic. We then further selected those peaks that were near genes that are induced in cic wts discs compared with wild-type. These strict criteria gave us a list of 19 high-confidence Cic target genes (Figure S2C). Strikingly, this set contained many regula-tors of the Ras pathway: the Spitz (Spi) ligand, and the negative

feedback regulators Aos, Sty, Nf1, and Sulfated (Sulf1) (Butchar et al., 2012). Hence, Cic is a key factor for feedback regulation of Ras signaling.

Next, we asked which factors might regulate the expression of these 19 Cic target genes using iRegulon. As expected, iRegulon identified the Cic motif as the top hit (NES = 7.3). In addition, regulatory regions of Cic target genes were also enriched for Pnt (NES = 4.5) and Stat92E (NES = 4.4) binding motifs (Figure 5B), similar to the predictions for synergistically induced genes. Indeed, 7 of the 19 Cic target genes were part of the synergistically induced gene set. These were the two known Cic targets pnt and aos; three other Ras pathway genes sty, nf1, and sulf1; leucine-rich tendon-specific protein (lrt); and brinker (brk). Therefore, induction of genes that are nor-mally repressed by Cic is the main feature of our synergistic network and at least seven of our synergistic target genes are direct Cic targets.

The finding that synergistically regulated genes are highly enriched for Cic target genes is striking, as it shows that the repressor function of Cic on its target genes is dependent on the level of Yki activity. Thus, while Cic represses the expression of Ras target genes, loss of this brake needs to be combined with activation of Yki-Sd to strongly induce their expression. This then prompted the question of whether the Yki-Sd complex directly regulates Cic target genes.

Sd and Cic Do Not Compete for DNA Binding

Intriguingly, the consensus DNA binding sequences of Sd (CATTCC) and Cic (CATT(C/G)A) are very similar and differ only at one position. Hence, Sd may directly compete with Cic for binding to regulatory sequences. We tested this hypothesis using the ChIP-nexus data for Cic and also performed ChIP-nexus for Sd. Combining ChIP-nexus signal with motif enrichment identified 800 regions bound by Sd in the genome of wing disc cells. Strikingly, we did not find binding sites that were bound by both Sd and Cic in wild-type wing discs. We then compared Sd binding between *wts* and *cic wts* mutant discs to ask whether Sd now occupies more sites. However, we did not detect new Sd peaks where Cic normally binds. Therefore, Sd does not regulate Cic target genes by competing with Cic for binding the DNA.

We also tested whether Cic can regulate Sd target genes by searching for Cic peaks in their regulatory regions. We did not find any Cic binding in the prominent Yki-Sd target genes *DIAP1*, *ex*, *wts*, *ft*, *ds*, *fj*, or *ilp8*. On the other hand, these regulatory regions were enriched for Sd motifs and had Sd binding as expected. In agreement with these findings, the expression of Yki-Sd target genes were induced at comparable levels in *wts* and *cic wts* mutant discs (Figure 4B), supporting the conclusion that Cic does not regulate the expression of Yki target genes. Therefore, we conclude that Sd and Cic do not affect each other's ability to bind to target DNA *in vivo*, and their binding motifs, despite only a single nucleotide difference, are clearly distinct.

JAK-STAT Signaling and Pnt Contribute to the Synergistic Overgrowth

iRegulon found no enrichment for Sd binding sites within our synergistic gene set. However, in addition to the Cic motif, this gene set was enriched for Pnt and Stat92E binding sites. Stat92E is the transcription factor of the JAK-STAT pathway, another important pathway in tumorigenesis (Amoyel et al., 2014; Zoranovic et al., 2013). Twenty-one of our 46 synergistic genes, including Pnt itself, are predicted to be regulated by Pnt, Cic, and Stat92E together (Figure 5A). More than half of our synergistic genes (27/46) had binding sites for at least two out of these three factors (Figure 5A). Therefore, we tested the importance of Pnt and Stat92E for the synergistic overgrowth.

First, we found that the ligands of the JAK-STAT pathway, the Unpaired cytokines Upd1 (also known as os), Upd2, and Upd3 are highly upregulated (2.1-, 2.6-, and 2.4-fold, respectively) in day-5 *wts* mutant discs (Figure 5C). Upd levels stayed high in day-9 *wts* discs and were further upregulated in *cic wts* double-mutant discs (3-, 6.18-, and 4.5-fold, respectively) (Figure 5C). Hence, having upregulated Upd ligand expression, JAK-STAT signaling is likely more active in *wts* and *cic wts* mutant cells. JAK-STAT signaling is frequently implicated in

human cancer and is commonly induced in *Drosophila* tumor models (Atkins et al., 2016; Davie et al., 2015; Wu et al., 2010). We then tested whether JAK-STAT activation is important for the synergistic overgrowth of *cic wts* mutants by expressing an inhibitor of the pathway, Socs36E (Stec et al., 2013), in our synergistic background (activated EGFR expression in *ex*). Co-expression of Socs36E efficiently suppressed the overgrowth phenotype in both wing and eye discs (Figures 5F and 5G versus 5D and 5E). Notably, the expression of the Upd genes is regulated by the Yki-Sd complex (Bunker et al., 2015), and we found ChIP-nexus peaks and corresponding motifs for both Sd and Cic near the *upd* genes (Figure S2D). Altogether, these results show that the transcriptional regulation of the Upd genes and the activation of JAK-STAT signaling is an important contributor to the synergy between the Hippo and Ras pathways.

We then used the same assay to test the contribution of Pnt upregulation to the synergistic phenotype. We constructed a stock where *UAS-pnt-RNAi* is under the control of the *dpp-Gal4* driver. These flies are viable, fertile, and only have mild venation defects on their wings (not shown), suggesting that Pnt function is only slightly reduced but largely intact in this background. However, this mild downregulation of Pnt activity was sufficient to prevent the development of fully fledged synergistic overgrowth. Discs that expressed *pnt-RNAi* in addition to activated EGFR in an *ex* mutant background did not display the full-grown synergistic overgrowth phenotype (Figures 5H–5J). Therefore, high Pnt levels are important for the synergistic overgrowth obtained when both Ras and the Hippo pathways are manipulated.

Yki-Sd Controls the Expression of the Ras Pathway Transcription Factors Pointed and Capicua

Having established that the network predicted by iRegulon is indeed driving the synergistic growth, and that Yki-Sd can influence this network via induction of Upd transcription, we asked whether Yki-Sd could also regulate the other nodes of the network, Pnt and Cic.

We first had a closer look at the regulation of Pnt. The PntP2 isoform is known to be activated by MAPK phosphorylation and drives the expression of PntP1 in eye discs (Shwartz et al., 2013). In addition, Cic negatively regulates Pnt expression in intestinal stem cells (Jin et al., 2015). To characterize its potential regulation by Hippo signaling, we generated antibodies against Pnt, which detected a pattern identical to dpERK and complementary to Cic in the wing and eye discs (Figures 6A, 6B, S3A, and S3B). Removal of Cic was sufficient to derepress Pnt expression in wild-type and *ex* mutant cells (Figures 6C, 6C′, S3F, and S3F′). Since *cic wts* mutant clones occupy large areas, Pnt was expressed widely and lost all pattern in *cic wts* discs (Figures S3G and S3G′). These data confirm a tight regulation of Pnt expression by Ras signaling and establish Cic as an important regulator of *pnt* expression in imaginal discs. Direct regulation of Pnt by Cic is also strongly supported by our ChIP data. Of the 100 top Cic peaks in the genome of wing disc cells, seven were in the *pnt* region and corresponded to Cic motifs (Figure 6D, Cic ChIP signal is shown in red; Sd ChIP signal is shown in blue). Furthermore, the RNA-seq data show that transcription of *pnt* is induced when the repressor Cic is removed (Figure 5C). Notably, RNA levels of *pnt* are further increased in *cic wts* double-mutant
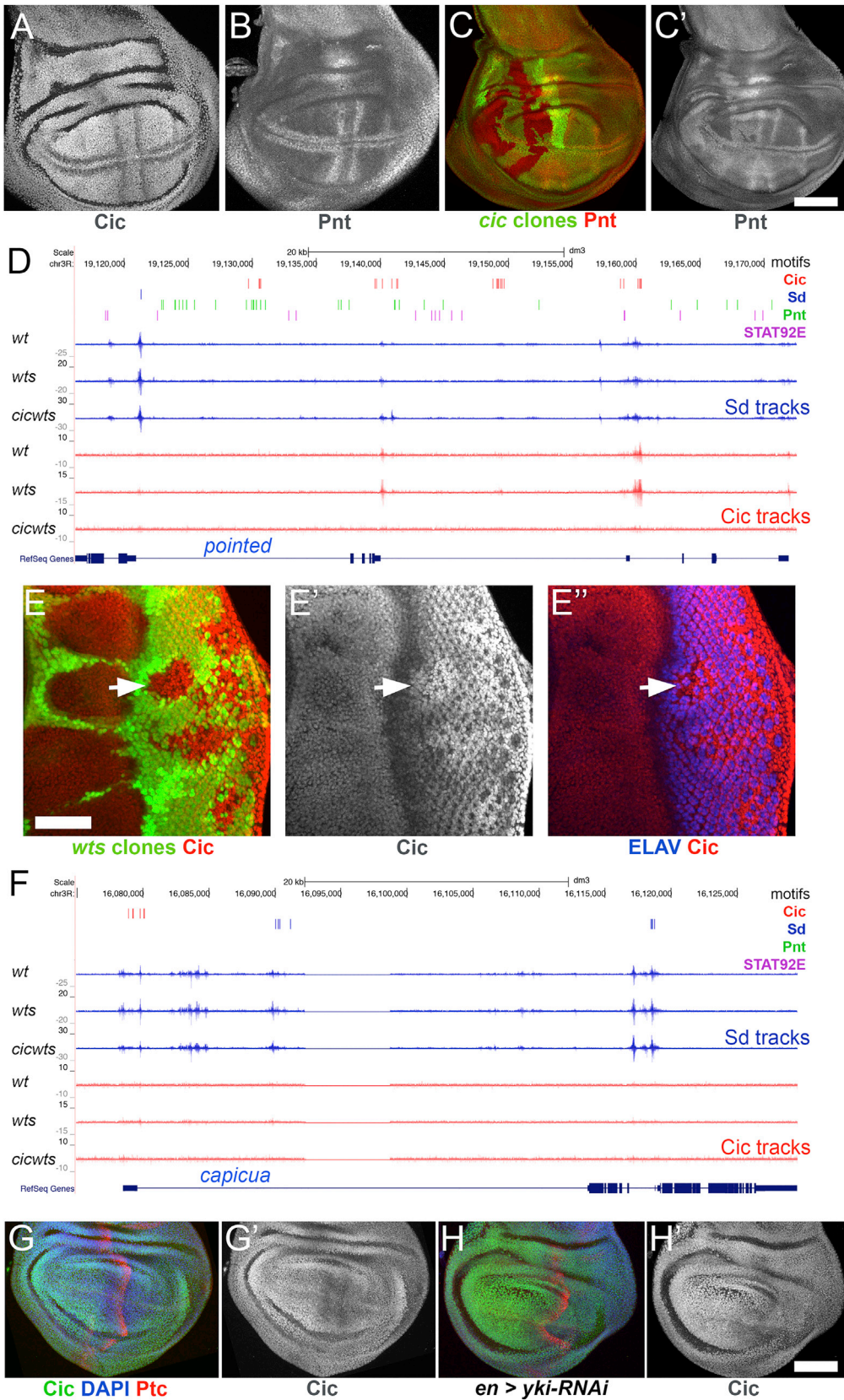
(legend on next page)

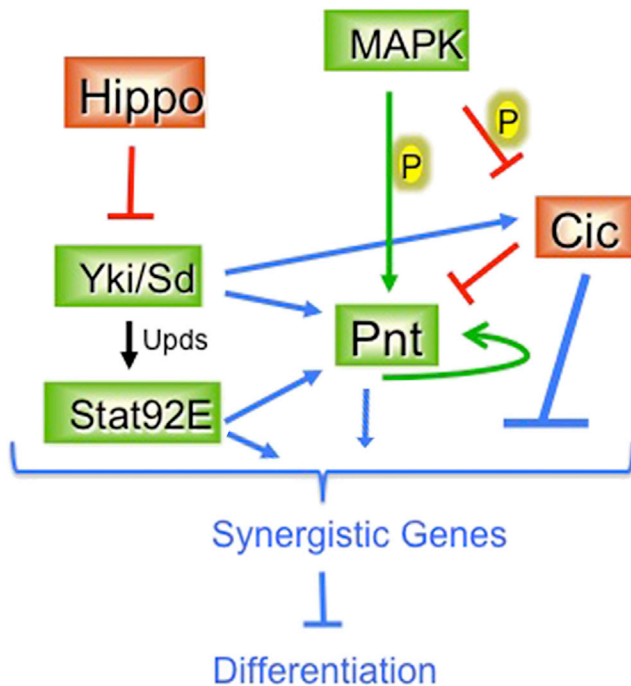Hippo and Cic provide brakes that prevent transformation

Figure 7. Model of the Transcriptional Interaction between the Hippo and Ras Pathways

The Hippo pathway effectors Yki-Sd regulate the expression of the Pnt and Cic transcription factors of the Ras pathway. The induction of Pnt regulates the sensitivity of a cell to Ras signaling, while the induction of Cic increases the threshold required for productive output. As a result, Cic target genes and synergy are only fully activated when Cic is removed and Yki is simultaneously activated. Thus, the activity of the Hippo pathway together with the repressor Cic provide parallel brakes that limit Ras signaling output and prevent hyperproliferation and cellular transformation. Blue highlights the interactions revealed in this study.

See also Figure S5.

discs, although there is no increase in *wts* single mutants (Figure 5C). In fact, *pnt* is expressed at lower levels in *wts* and *ex* mutant discs (Figures 5C and S3E), probably due to higher Cic levels. Therefore there must be another, positive input into *pnt* expression that depends on Yki-Sd (Figure 5A). Indeed, our ChIP-nexus detected a strong Sd peak containing an Sd motif (blue) in the *pnt* gene, which is also enriched for Pnt (green) and Stat92E (purple) binding sites (Figure 6D). We conclude that Cic, Yki-Sd, Stat92E, and Pnt itself control *pnt* transcription, and that repression by Cic is dominant over the activating inputs.

Finally, we investigated whether Cic is a Sd target gene. We found multiple Sd ChIP-nexus peaks with corresponding Sd binding motifs in the *cic* gene region (Figure 6F). However, *cic* RNA levels, as well as Cic protein levels, were only slightly higher in *wts* mutant wing discs (Figure 5C, 1.1-fold in day-5 discs and 1.23-fold in day-9 discs). On the other hand, Cic accumulation was obvious in *wts* clones, in eye discs posterior to the morphogenetic furrow and in between the clusters of differentiating photoreceptor cells (Figures 6E and 6E″), where Cic is normally present at low levels (Figure S3B). Cic is expressed at high levels and uniformly in the wing discs, except for the cells where MAPK leads to its degradation (Figure 6A). We thus hypothesized that Yki-Sd are required for the high uniform Cic expression. Indeed, knockdown of Yki in the posterior half of wing discs reduced Cic levels (Figures 6G–6H′). Hence, induction of Cic transcription by Yki-Sd increases the threshold of Ras activity that is required to induce its target genes.

DISCUSSION

The main conclusion from our study is that Hippo activity determines the outcome of Ras signaling. In our model, combined action of Hippo signaling and the repressor Cic prevents excessive proliferation and allows differentiation by keeping off a set of key target genes (Figure 7). Cic suppresses many of these genes directly, and Hippo signaling prevents their full activation, at least partially, by keeping both JAK/STAT activity and Pnt levels low. This model is based on three key observations. First, we found that activated Ras signaling has different outcomes in wild-type discs versus *ex* mutant discs. While hyperactivation of Ras signaling in a wild-type disc promotes cellular differentiation, Ras activation combined with loss of *ex* drives aggressive hyperproliferation. Second, we defined a set of synergistic genes that were strongly induced only when the repressor Cic was removed and Yki was simultaneously activated. These genes were predicted to be regulated by Cic, Pnt, and Stat92E. Indeed, we confirmed that high Pnt levels and JAK/STAT activity contributed to the synergistic overgrowth phenotype. Lastly, we found that the Hippo pathway transcription factor Sd directly regulates the expression of the JAK/STAT ligands and the Ras signaling transcription factors Cic and Pnt. When Hippo signaling and Cic are simultaneously inhibited, the synergistic genes and the Yki targets are expressed at high levels, paving the way to cellular transformation.

We defined a small set of direct Cic target genes in wing discs. Identification of many feedback regulators of Ras signaling among direct Cic targets emphasizes the central role of this protein in controlling Ras output despite the weak phenotypic

Figure 6. Pointed and Cic Are Direct Yki-Sd Targets

(A and B) Cic and Pnt expression patterns, detected by antibody stainings, in late third-instar wing discs.

(C and C′) Pnt is derepressed in *cic* mutant clones.

(D and F) ChIP-nexus tracks in *pnt* (D) and *cic* (F) genomic regions obtained by overlaying tracks from experimental triplicates. Blue and red tracks correspond to Sd and Cic ChIP data, respectively. Predicted binding motifs for Cic (red), Sd (blue), Pnt (green), and Stat92E (purple) are shown above the tracks.

(E–E″) Cic (red in E and E″, gray in E′) and ELAV (blue in E″) antibody staining in discs with *wts*[149] mutant clones marked by the absence of GFP (green in E) is shown. Cic protein accumulates in interommatidial cells (arrows).

(G–H′) Knocking down *yki* in the posterior compartment leads to a reduction in the compartment size and Cic levels. High, uniform Cic levels require Yki input. Scale bars in (C′), (E), and (H′), 100 μm (all images are shown on the same scale).

Genotypes: (C): *y w hsflp/y w; FRT82B ubiGFP[nls]/FRT82B cic[Q474X]*; (E): *y w hsflp/y w; FRT82B ubiGFP[nls]/FRT82B wts[149]*; (G): *y w; en-Gal4/+*; (H): *y w; en-Gal4/+; UAS-Yki-RNAi/+*. See also Figure S3.

consequences of its removal. Notably, Cic expression is complementary to that of the other two transcription factors of Ras signaling, Pnt and Yan (Figures S3A–S3C). Indeed, Cic controls Pnt transcription in multiple tissues, but our RNA-seq and ChIP-nexus data on wing discs suggest that Cic does not regulate Yan.

Our data reveal a fundamental interaction between the Ras and Hippo pathways occurring at the level of their downstream transcription factors. Other points of crosstalk have been reported in the literature. Most prominently, MAPK was suggested to phosphorylate and activate the LIM-domain protein Ajuba, a negative regulator of the Wts kinase (Reddy and Irvine, 2013). Similarly, oncogenic Ras can induce Yap activation (Reddy and Irvine, 2013; Hong et al., 2014). We confirmed that overexpression of constitutively active EGFR or Ras induced the expression of the Yki-regulated reporter gene *ex-lacZ* (Figures S4A and S4B). Surprisingly however, this was not a general effect and was dependent on the position of the clone. Thus the effect of Ras hyperactivation on the Hippo pathway depends on the fate of a cell. Likewise, only a fraction of patients with activating mutations in Ras have elevated YAP levels paralleling the context dependency that we observed in discs (Lin et al., 2015). Unlike activation of Ras, loss of *cic* did not induce Yki activity. Notably, this was true in a wild-type background and in *ex* and *wts* mutant backgrounds where loss of *cic* caused synergistic overgrowth (Figures S4C–S4F). Two conclusions follow from these results. First, Ras signaling crosses over to the Hippo pathway only upstream of Cic, consistent with the model whereby MAPK regulates the activity of Ajuba (Reddy and Irvine, 2013). Second, the synergy between Ras and Hippo signaling cannot depend on the regulation of Hippo pathway activity by Ras signaling, because loss of *cic* synergized with loss of *wts* in growth control even though Cic does not affect Yki activity. Thus, the synergy between the Hippo and Ras pathways is not due to a general activation of Yki in response to loss of Cic. Rather, we show that the synergy is due to hyperactivation of the Ras signaling output, which is under direct Yki-Sd control. Therefore, there are at least two points of crosstalk between the two pathways: one upstream of Cic via Ajuba and another at the level of transcription factors as described here.

Strikingly, in the *cic wts* double-mutant discs, the activities of the other major developmental pathways are reduced: Dpp, Hh, N, and Wg signaling activity readouts are expressed at low levels, suggesting a block in the differentiation program (Figure S5A). Activation of two key Cic target genes, Sulf1 and Brk, are likely to account for this observation. Sulf1 encodes an extracellular protein from the endosulfatase family that regulates the amount and pattern of sulfate groups on heparan sulfate proteoglycans (HSPGs). HSPGs in turn play major roles in morphogen distribution and patterning (Yan and Lin, 2009). Accordingly, Sulf1 was linked to dampening the activity of Wg and Hh signaling pathways (Kleinschmit et al., 2013; You et al., 2011; Wojcinski et al., 2011). Brk, the default repressor of Dpp signaling (Affolter and Basler, 2007), is also a direct Cic target and is highly induced in *cic wts* cells. As a result of the action of Sulf1, Brk, and potentially others, we see a block in differentiation signature in *cic wts* double-mutant cells (Figure S5A). In these cells the readout for Ras signaling is highly upregulated, and simultaneously Dpp, N, Wg, and Hh pathways are downregulated. Consequently, *cic*

wts cells lose their differentiation potential and proliferate aggressively (Figure S5B). Therefore, combined mutations in Hippo and Ras pathways are especially dangerous as both brakes that dampen the transformation potential of a cell are removed (Figure 7). We show that Cic and its targets are central to Ras-driven tumorigenesis and the choice between differentiation and proliferation. Activation of Yki/YAP along with Cic degradation switches the response of a cell from differentiation to proliferation by allowing full activation of Cic targets.

Our analysis of the mechanism by which Hippo and Ras synergize to produce massive tissue overproliferation in flies is likely to be relevant to tumor formation in vertebrates. Recent work indicates that if activation of Ras or Raf is coupled with amplification of the YAP region, the resulting carcinomas are more aggressive and resistant to MEK and Raf inhibitors (Lin et al., 2015). It has also been shown that mutations in Nf2, an upstream regulator of Hippo, cooperate with activating Ras mutations in a mouse model of thyroid cancer and that co-expression of Ras and YAP lead to brain tumor formation in zebrafish (Garcia-Rendueles et al., 2015; Mayrhofer et al., 2017). Lastly, the regulation of Cic transcription by Yki/Sd may be conserved as CIC is induced in the mouse liver upon YAP overexpression (Yimlamai et al., 2014). These findings bring forth the conservation of tumor-suppressor pathway structures and underline the need for a mechanistic understanding such as the one exposed here. Our results argue that the transcriptional output of Ras signaling is under Hippo control and that Cic targets can only be fully activated when Yki/YAP is active (Figure 7). Requiring Yki activation and simultaneous removal of Cic for full induction, such "synergy genes" may represent attractive drug targets.

STAR★METHODS

Detailed methods are provided in the online version of this paper and include the following:

- KEY RESOURCES TABLE
- CONTACT FOR REAGENT AND RESOURCE SHARING
- EXPERIMENTAL MODEL AND SUBJECT DETAILS
- METHOD DETAILS
  - Immunohistochemistry
  - Antibody Production
  - RNA-seq Sample Preparation and Sequencing
  - Isolation of Chromatin from Imaginal Discs
  - ChIP-nexus
- QUANTIFICATION AND STATISTICAL ANALYSIS
  - iRegulon Normalized Enrichment Scores (NES)
  - RNA-seq Analysis
  - ChIP-nexus Analysis
- DATA AND SOFTWARE AVAILABILITY

SUPPLEMENTAL INFORMATION

Supplemental Information includes five figures and can be found with this article online at http://dx.doi.org/10.1016/j.devcel.2017.08.013.

AUTHOR CONTRIBUTIONS

REFERENCES

Affolter, M., and Basler, K. (2007). The decapentaplegic morphogen gradient: from pattern formation to growth regulation. Nat. Rev. Genet. *8*, 663–674.

Amoyel, M., Anderson, A.M., and Bach, E.A. (2014). JAK/STAT pathway dysregulation in tumors: a *Drosophila* perspective. Semin. Cell Dev. Biol. *28*, 96–103.

Anders, S., Pyl, P.T., and Huber, W. (2015). HTSeq—a Python framework to work with high-throughput sequencing data. Bioinformatics *31*, 166–169.

Atkins, M., Potier, D., Romanelli, L., Jacobs, J., Mach, J., Hamaratoglu, F., Aerts, S., and Halder, G. (2016). An ectopic network of transcription factors regulated by hippo signaling drives growth and invasion of a malignant tumor model. Curr. Biol. *26*, 2101–2113.

Ballester, R., Marchuk, D., Boguski, M., Saulino, A., Letcher, R., Wigler, M., and Collins, F. (1990). The NF1 locus encodes a protein functionally related to mammalian GAP and yeast IRA proteins. Cell *63*, 851–859.

Barry, E.R., and Camargo, F.D. (2013). The Hippo superhighway: signaling crossroads converging on the Hippo/Yap pathway in stem cells and development. Curr. Opin. Cell Biol. *25*, 247–253.

Boone, E., Colombani, J., Andersen, D.S., and Léopold, P. (2016). The Hippo signalling pathway coordinates organ growth and limits developmental variability by controlling dilp8 expression. Nat. Commun. *7*, 13505.

Brand, A.H., and Perrimon, N. (1994). Raf acts downstream of the EGF receptor to determine dorsoventral polarity during *Drosophila* oogenesis. Genes Dev. *8*, 629–639.

Brumby, A.M., and Richardson, H.E. (2003). Scribble mutants cooperate with oncogenic Ras or Notch to cause neoplastic overgrowth in *Drosophila*. EMBO J. *22*, 5769–5779.

Buchberg, A.M., Cleveland, L.S., Jenkins, N.A., and Copeland, N.G. (1990). Sequence homology shared by neurofibromatosis type-1 gene and IRA-1 and IRA-2 negative regulators of the RAS cyclic AMP pathway. Nature *347*, 291–294.

Bunker, B.D., Nellimoottil, T.T., Boileau, R.M., Classen, A.K., and Bilder, D. (2015). The transcriptional response to tumorigenic polarity loss in *Drosophila*. Elife *4*, e03189.

Burgess, A.W. (2008). EGFR family: structure physiology signalling and therapeutic targets. Growth Factors *26*, 263–274.

Butchar, J.P., Cain, D., Manivannan, S.N., McCue, A.D., Bonanno, L., Halula, S., Truesdell, S., Austin, C.L., Jacobsen, T.L., and Simcox, A. (2012). New negative feedback regulators of Egfr signaling in *Drosophila*. Genetics *191*, 1213–1226.

Casci, T., Vinós, J., and Freeman, M. (1999). Sprouty, an intracellular inhibitor of Ras signaling. Cell *96*, 655–665.

Chabu, C., Li, D.M., and Xu, T. (2017). EGFR/ARF6 regulation of Hh signalling stimulates oncogenic Ras tumour overgrowth. Nat. Commun. *8*, 14688.

Colombani, J., Polesello, C., Josué, F., and Tapon, N. (2006). Dmp53 activates the Hippo pathway to promote cell death in response to DNA damage. Curr. Biol. *16*, 1453–1458.

Davie, K., Jacobs, J., Atkins, M., Potier, D., Christiaens, V., Halder, G., and Aerts, S. (2015). Discovery of transcription factors and regulatory regions driving in vivo tumor development by ATAC-seq and FAIRE-seq open chromatin profiling. PLoS Genet. *11*, e1004994.

Dopazo, J., and Carazo, J.M. (1997). Phylogenetic reconstruction using an unsupervised growing neural network that adopts the topology of a phylogenetic tree. J. Mol. Evol. *44*, 226–233.

Feng, J., Liu, T., and Zhang, Y. (2011). Using MACS to identify peaks from ChIP-seq data. Curr. Protoc. Bioinformatics *Chapter 2*. Unit 2.14.

Forbes, S.A., Beare, D., Gunasekaran, P., Leung, K., Bindal, N., Boutselakis, H., Ding, M., Bamford, S., Cole, C., Ward, S., et al. (2015). COSMIC: exploring the world's knowledge of somatic mutations in human cancer. Nucleic Acids Res. *43* (Database issue), D805–D811.

Garcia-Rendueles, M.E., Ricarte-Filho, J.C., Untch, B.R., Landa, I., Knauf, J.A., Voza, F., Smith, V.E., Ganly, I., Taylor, B.S., Persaud, Y., et al. (2015). NF2 loss promotes oncogenic RAS-induced thyroid cancers via YAP-dependent transactivation of RAS proteins and sensitizes them to MEK inhibition. Cancer Discov. *5*, 1178–1193.

Garoia, F., Grifoni, D., Trotta, V., Guerra, D., Pezzoli, M.C., and Cavicchi, S. (2005). The tumor suppressor gene fat modulates the EGFR-mediated proliferation control in the imaginal tissues of *Drosophila* melanogaster. Mech. Dev. *122*, 175–187.

Gaujoux, R., and Seoighe, C. (2010). A flexible R package for nonnegative matrix factorization. BMC Bioinformatics *11*, 367.

Glise, B., Miller, C.A., Crozatier, M., Halbisen, M.A., Wise, S., Olson, D.J., Vincent, A., and Blair, S.S. (2005). Shifted, the *Drosophila* ortholog of Wnt inhibitory factor-1, controls the distribution and movement of Hedgehog. Dev. Cell *8*, 255–266.

Golembo, M., Schweitzer, R., Freeman, M., and Shilo, B.Z. (1996). Argos transcription is induced by the *Drosophila* EGF receptor pathway to form an inhibitory feedback loop. Development *122*, 223–230.

Gorfinkiel, N., Sierra, J., Callejo, A., Ibañez, C., and Guerrero, I. (2005). The *Drosophila* ortholog of the human Wnt inhibitor factor Shifted controls the diffusion of lipid-modified Hedgehog. Dev. Cell *8*, 241–253.

Grusche, F.A., Richardson, H.E., and Harvey, K.F. (2010). Upstream regulation of the hippo size control pathway. Curr. Biol. *20*, R574–R582.

Halder, G., and Johnson, R.L. (2011). Hippo signaling: growth control and beyond. Development *138*, 9–22.

Hamaratoglu, F., Willecke, M., Kango-Singh, M., Nolo, R., Hyun, E., Tao, C., Jafar-Nejad, H., and Halder, G. (2006). The tumour-suppressor genes NF2/Merlin and Expanded act through Hippo signalling to regulate cell proliferation and apoptosis. Nat. Cell Biol. *8*, 27–36.

Hamaratoglu, F., de Lachapelle, A.M., Pyrowolakis, G., Bergmann, S., and Affolter, M. (2011). Dpp signaling activity requires pentagone to scale with

tissue size in the growing *Drosophila* wing imaginal disc. PLoS Biol. *9*, e1001182.

Hariharan, I.K. (2015). Organ size control: lessons from *Drosophila*. Dev. Cell *34*, 255–265.

Harvey, K.F., Zhang, X., and Thomas, D.M. (2013). The Hippo pathway and human cancer. Nat. Rev. Cancer *13*, 246–257.

He, Q., Johnston, J., and Zeitlinger, J. (2015). ChIP-nexus enables improved detection of in vivo transcription factor binding footprints. Nat. Biotechnol. *33*, 395–401.

Herrero, J., Valencia, A., and Dopazo, J. (2001). A hierarchical unsupervised growing neural network for clustering gene expression patterns. Bioinformatics *17*, 126–136.

Hong, X., Nguyen, H.T., Chen, Q., Zhang, R., Hagman, Z., Voorhoeve, P.M., and Cohen, S.M. (2014). Opposing activities of the Ras and Hippo pathways converge on regulation of YAP protein turnover. EMBO J. *33*, 2447–2457.

Ikmi, A., Gaertner, B., Seidel, C., Srivastava, M., Zeitlinger, J., and Gibson, M.C. (2014). Molecular evolution of the Yap/Yorkie proto-oncogene and elucidation of its core transcriptional program. Mol. Biol. Evol. *31*, 1375–1390.

Imrichová, H., Hulselmans, G., Atak, Z.K., Potier, D., and Aerts, S. (2015). i-cisTarget 2015 update: generalized cis-regulatory enrichment analysis in human, mouse and fly. Nucleic Acids Res. *43* (W1), W57–W64.

Janky, R., Verfaillie, A., Imrichová, H., Van de Sande, B., Standaert, L., Christiaens, V., Hulselmans, G., Herten, K., Naval Sanchez, M., Potier, D., et al. (2014). iRegulon: from a gene list to a gene regulatory network using large motif and track collections. PLoS Comput. Biol. *10*, e1003731.

Jiménez, G., Shvartsman, S.Y., and Paroush, Z. (2012). The Capicua repressor–a general sensor of RTK signaling in development and disease. J. Cell Sci. *125* (Pt 6), 1383–1391.

Jin, Y., Ha, N., Forés, M., Xiang, J., Gläßer, C., Maldera, J., Jiménez, G., and Edgar, B.A. (2015). EGFR/Ras signaling controls *Drosophila* intestinal stem cell proliferation via capicua-regulated genes. PLoS Genet. *11*, e1005634.

Justice, R.W., Zilian, O., Woods, D.F., Noll, M., and Bryant, P.J. (1995). The *Drosophila* tumor suppressor gene warts encodes a homolog of human myotonic dystrophy kinase and is required for the control of cell shape and proliferation. Genes Dev. *9*, 534–546.

Kagey, J.D., Brown, J.A., and Moberg, K.H. (2012). Regulation of Yorkie activity in *Drosophila* imaginal discs by the Hedgehog receptor gene patched. Mech. Dev. *129*, 339–349.

Kandoth, C., McLellan, M.D., Vandin, F., Ye, K., Niu, B., Lu, C., Xie, M., Zhang, Q., McMichael, J.F., Wyczalkowski, M.A., et al. (2013). Mutational landscape and significance across 12 major cancer types. Nature *502*, 333–339.

Karaman, R., and Halder, G. (2017). Cell junctions in Hippo signaling. Cold Spring Harb. Perspect. Biol. http://dx.doi.org/10.1101/cshperspect.a028753.

Kim, D., Pertea, G., Trapnell, C., Pimentel, H., Kelley, R., and Salzberg, S.L. (2013). TopHat2: accurate alignment of transcriptomes in the presence of insertions, deletions and gene fusions. Genome Biol. *14*, R36.

Kleinschmit, A., Takemura, M., Dejima, K., Choi, P.Y., and Nakato, H. (2013). *Drosophila* heparan sulfate 6-O-endosulfatase Sulf1 facilitates wingless (Wg) protein degradation. J. Biol. Chem. *288*, 5081–5089.

Koontz, L.M., Liu-Chittenden, Y., Yin, F., Zheng, Y., Yu, J., Huang, B., Chen, Q., Wu, S., and Pan, D. (2013). The Hippo effector Yorkie controls normal tissue growth by antagonizing scalloped-mediated default repression. Dev. Cell *25*, 388–401.

Lee, K.P., Lee, J.H., Kim, T.S., Kim, T.H., Park, H.D., Byun, J.S., Kim, M.C., Jeong, W.I., Calvisi, D.F., Kim, J.M., and Lim, D.S. (2010). The Hippo-Salvador pathway restrains hepatic oval cell proliferation, liver size, and liver tumorigenesis. Proc. Natl. Acad. Sci. USA *107*, 8248–8253.

Legoff, L., Rouault, H., and Lecuit, T. (2013). A global pattern of mechanical stress polarizes cell divisions and cell shape in the growing *Drosophila* wing disc. Development *140*, 4051–4059.

Lemmon, M.A., and Schlessinger, J. (2010). Cell signaling by receptor tyrosine kinases. Cell *141*, 1117–1134.

Lin, L., Sabnis, A.J., Chan, E., Olivas, V., Cade, L., Pazarentzos, E., Asthana, S., Neel, D., Yan, J.J., Lu, X., et al. (2015). The Hippo effector YAP promotes resistance to RAF- and MEK-targeted cancer therapies. Nat. Genet. *47*, 250–256.

Love, M.I., Huber, W., and Anders, S. (2014). Moderated estimation of fold change and dispersion for RNA-seq data with DESeq2. Genome Biol. *15*, 550.

Lu, L., Li, Y., Kim, S.M., Bossuyt, W., Liu, P., Qiu, Q., Wang, Y., Halder, G., Finegold, M.J., Lee, J.S., and Johnson, R.L. (2010). Hippo signaling is a potent in vivo growth and tumor suppressor pathway in the mammalian liver. Proc. Natl. Acad. Sci. USA *107*, 1437–1442.

Ma, X., Chen, Y., Xu, W., Wu, N., Li, M., Cao, Y., Wu, S., Li, Q., and Xue, L. (2015). Impaired Hippo signaling promotes Rho1-JNK-dependent growth. Proc. Natl. Acad. Sci. USA *112*, 1065–1070.

Mao, Y., Tournier, A.L., Hoppe, A., Kester, L., Thompson, B.J., and Tapon, N. (2013). Differential proliferation rates generate patterns of mechanical tension that orient tissue growth. EMBO J. *32*, 2790–2803.

Martin, G.A., Viskochil, D., Bollag, G., McCabe, P.C., Crosier, W.J., Haubruck, H., Conroy, L., Clark, R., O'Connell, P., and Cawthon, R.M. (1990). The GAP-related domain of the neurofibromatosis type 1 gene product interacts with ras p21. Cell *63*, 843–849.

Marygold, S.J., Coelho, C.M., and Leevers, S.J. (2005). Genetic analysis of RpL38 and RpL5, two minute genes located in the centric heterochromatin of chromosome 2 of *Drosophila melanogaster*. Genetics *169*, 683–695.

Mayrhofer, M., Gourain, V., Reischl, M., Affaticati, P., Jenett, A., Joly, J.S., Benelli, M., Demichelis, F., Poliani, P.L., Sieger, D., and Mione, M. (2017). A novel brain tumour model in zebrafish reveals the role of YAP activation in MAPK- and PI3K-induced malignant growth. Dis. Model. Mech. *10*, 15–28.

Morata, G., and Ripoll, P. (1975). Minutes: mutants of *Drosophila* autonomously affecting cell division rate. Dev. Biol. *42*, 211–221.

Neto-Silva, R.M., de Beco, S., and Johnston, L.A. (2010). Evidence for a growth-stabilizing regulatory feedback mechanism between Myc and Yorkie, the *Drosophila* homolog of Yap. Dev. Cell *19*, 507–520.

Okamoto, N., Nakamori, R., Murai, T., Yamauchi, Y., Masuda, A., and Nishimura, T. (2013). A secreted decoy of InR antagonizes insulin/IGF signaling to restrict body growth in *Drosophila*. Genes Dev. *27*, 87–97.

Pagliarini, R.A., and Xu, T. (2003). A genetic screen in *Drosophila* for metastatic behavior. Science *302*, 1227–1231.

Pan, D. (2007). Hippo signaling in organ size control. Genes Dev. *21*, 886–897.

Pan, D. (2010). The hippo signaling pathway in development and cancer. Dev. Cell *19*, 491–505.

Park, G.S., Oh, H., Kim, M., Kim, T., Johnson, R.L., Irvine, K.D., and Lim, D.S. (2016). An evolutionarily conserved negative feedback mechanism in the Hippo pathway reflects functional difference between LATS1 and LATS2. Oncotarget *7*, 24063–24075.

Pearson, H.B., Perez-Mancera, P.A., Dow, L.E., Ryan, A., Tennstedt, P., Bogani, D., Elsum, I., Greenfield, A., Tuveson, D.A., Simon, R., and Humbert, P.O. (2011). SCRIB expression is deregulated in human prostate cancer, and its deficiency in mice promotes prostate neoplasia. J. Clin. Invest. *121*, 4257–4267.

Piccolo, S., Dupont, S., and Cordenonsi, M. (2014). The biology of YAP/TAZ: hippo signaling and beyond. Physiol. Rev. *94*, 1287–1312.

Queenan, A.M., Ghabrial, A., and Schüpbach, T. (1997). Ectopic activation of torpedo/Egfr, a *Drosophila* receptor tyrosine kinase, dorsalizes both the eggshell and the embryo. Development *124*, 3871–3880.

Reddy, B.V., and Irvine, K.D. (2013). Regulation of Hippo signaling by EGFR-MAPK signaling through Ajuba family proteins. Dev. Cell *24*, 459–471.

Richardson, H.E., and Portela, M. (2017). Tissue growth and tumorigenesis in *Drosophila*: cell polarity and the Hippo pathway. Curr. Opin. Cell Biol. *48*, 1–9.

Roch, F., Jiménez, G., and Casanova, J. (2002). EGFR signalling inhibits Capicua-dependent repression during specification of *Drosophila* wing veins. Development *129*, 993–1002.

Saeed, A.I., Sharov, V., White, J., Li, J., Liang, W., Bhagabati, N., Braisted, J., Klapa, M., Currier, T., Thiagarajan, M., et al. (2003). TM4: a free, open-source

system for microarray data management and analysis. Biotechniques *34*, 374–378.

Schnidar, H., Eberl, M., Klingler, S., Mangelberger, D., Kasper, M., Hauser-Kronberger, C., Regl, G., Kroismayr, R., Moriggl, R., Sibilia, M., and Aberger, F. (2009). Epidermal growth factor receptor signaling synergizes with Hedgehog/GLI in oncogenic transformation via activation of the MEK/ERK/JUN pathway. Cancer Res. *69*, 1284–1292.

Scholz, H., Sadlowski, E., Klaes, A., and Klämbt, C. (1997). Control of midline glia development in the embryonic *Drosophila* CNS. Mech. Dev. *64*, 137–151.

Schweitzer, R., Howes, R., Smith, R., Shilo, B.Z., and Freeman, M. (1995). Inhibition of *Drosophila* EGF receptor activation by the secreted protein Argos. Nature *376*, 699–702.

Shilo, B.Z. (2014). The regulation and functions of MAPK pathways in *Drosophila*. Methods *68*, 151–159.

Shwartz, A., Yogev, S., Schejter, E.D., and Shilo, B.Z. (2013). Sequential activation of ETS proteins provides a sustained transcriptional response to EGFR signaling. Development *140*, 2746–2754.

Song, H., Mak, K.K., Topol, L., Yun, K., Hu, J., Garrett, L., Chen, Y., Park, O., Chang, J., Simpson, R.M., et al. (2010). Mammalian Mst1 and Mst2 kinases play essential roles in organ size control and tumor suppression. Proc. Natl. Acad. Sci. USA *107*, 1431–1436.

Stec, W., Vidal, O., and Zeidler, M.P. (2013). *Drosophila* SOCS36E negatively regulates JAK/STAT pathway signaling via two separable mechanisms. Mol. Biol. Cell *24*, 3000–3009.

Stemerdink, C., and Jacobs, J.R. (1997). Argos and Spitz group genes function to regulate midline glial cell number in *Drosophila* embryos. Development *124*, 3787–3796.

Tomasetti, C., Marchionni, L., Nowak, M.A., Parmigiani, G., and Vogelstein, B. (2015). Only three driver gene mutations are required for the development of lung and colorectal cancers. Proc. Natl. Acad. Sci. USA *112*, 118–123.

Tseng, A.S., Tapon, N., Kanda, H., Cigizoglu, S., Edelmann, L., Pellock, B., White, K., and Hariharan, I.K. (2007). Capicua regulates cell proliferation downstream of the receptor tyrosine kinase/ras signaling pathway. Curr. Biol. *17*, 728–733.

Uhlirova, M., and Bohmann, D. (2006). JNK- and Fos-regulated Mmp1 expression cooperates with Ras to induce invasive tumors in *Drosophila*. EMBO J. *25*, 5294–5304.

Vakiani, E., and Solit, D.B. (2011). KRAS and BRAF: drug targets and predictive biomarkers. J. Pathol. *223*, 219–229.

Wojcinski, A., Nakato, H., Soula, C., and Glise, B. (2011). DSulfatase-1 fine-tunes Hedgehog patterning activity through a novel regulatory feedback loop. Dev. Biol. *358*, 168–180.

Wu, M., Pastor-Pareja, J.C., and Xu, T. (2010). Interaction between Ras(V12) and scribbled clones induces tumour growth and invasion. Nature *463*, 545–548.

Xia, M., and Land, H. (2007). Tumor suppressor p53 restricts Ras stimulation of RhoA and cancer cell motility. Nat. Struct. Mol. Biol. *14*, 215–223.

Xu, G.F., Lin, B., Tanaka, K., Dunn, D., Wood, D., Gesteland, R., White, R., Weiss, R., and Tamanoi, F. (1990). The catalytic domain of the neurofibromatosis type 1 gene product stimulates ras GTPase and complements ira mutants of *S. cerevisiae*. Cell *63*, 835–841.

Xu, T., Wang, W., Zhang, S., Stewart, R.A., and Yu, W. (1995). Identifying tumor suppressors in genetic mosaics: the *Drosophila* lats gene encodes a putative protein kinase. Development *121*, 1053–1063.

Yan, D., and Lin, X. (2009). Shaping morphogen gradients by proteoglycans. Cold Spring Harb. Perspect. Biol. *1*, a002493.

Yang, L., and Baker, N.E. (2001). Role of the EGFR/Ras/Raf pathway in specification of photoreceptor cells in the *Drosophila* retina. Development *128*, 1183–1191.

Yang, L., and Baker, N.E. (2003). Cell cycle withdrawal, progression, and cell survival regulation by EGFR and its effectors in the differentiating *Drosophila* eye. Dev. Cell *4*, 359–369.

Yimlamai, D., Christodoulou, C., Galli, G.G., Yanger, K., Pepe-Mooney, B., Gurung, B., Shrestha, K., Cahan, P., Stanger, B.Z., and Camargo, F.D. (2014). Hippo pathway activity influences liver cell fate. Cell *157*, 1324–1338.

You, J., Belenkaya, T., and Lin, X. (2011). Sulfated is a negative feedback regulator of wingless in *Drosophila*. Dev. Dyn. *240*, 640–648.

Zanconato, F., Cordenonsi, M., and Piccolo, S. (2016). YAP/TAZ at the roots of cancer. Cancer Cell *29*, 783–803.

Zhou, D., Conrad, C., Xia, F., Park, J.S., Payer, B., Yin, Y., Lauwers, G.Y., Thasler, W., Lee, J.T., Avruch, J., and Bardeesy, N. (2009). Mst1 and Mst2 maintain hepatocyte quiescence and suppress hepatocellular carcinoma development through inactivation of the Yap1 oncogene. Cancer Cell *16*, 425–438.

Ziosi, M., Baena-López, L.A., Grifoni, D., Froldi, F., Pession, A., Garoia, F., Trotta, V., Bellosta, P., and Cavicchi, S. (2010). dMyc functions downstream of Yorkie to promote the supercompetitive behavior of hippo pathway mutant cells. PLoS Genet. *6*, e1001140.

Zoranovic, T., Grmai, L., and Bach, E.A. (2013). Regulation of proliferation, cell competition, and cellular growth by the *Drosophila* JAK-STAT pathway. JAKSTAT *2*, e25408.

STAR★METHODS

KEY RESOURCES TABLE

REAGENT or RESOURCE	SOURCE	IDENTIFIER
Antibodies		
m-β-gal	Promega	Z3781; RRID: AB_430877
r-ELAV	Developmental Studies Hybridoma Bank (DSHB)	7E8A10; RRID: AB_528218
m-Ptc	DSHB	Apa-1; RRID: AB_528441
m-Yan	DSHB	8B12H9; RRID: AB_531807
r-Ci	Robert A. Holmgren, Northwestern University	DSHB Cat# 2A1; RRID: AB_2109711
rb-Pnt	This paper	N/A
rb-Cic	This paper	N/A
gp-Cic	Tseng et al., 2007	RRID: AB_2569908
rb-Ex	Allen Laughon, University of Wisconsin-Madison	N/A
rb-Sd	Ikmi et al., 2014	RRID: AB_2568089
Deposited Data		
RNA-seq in wing imaginal discs. Triplicates of wt_d5, *cic*_d5, *wts*_d5, *wts*_d9, *cic wts*_d5, and *cic wts*_d9.	This paper	GEO: GSE96868
ChIP-Nexus-seq in wing imaginal discs - against Scalloped: 2 wt, 2 *wts*, 3 *cic wts* samples - against Capicua: 2 wt, 2 *wts*, 2 *cic wts* samples	This paper	GEO: GSE96868
Capicua expression in mouse livers	Yimlamai et al., 2014	GEO: GSE55560
Experimental Models: Organisms/Strains		
w; FRT40A ex^{e1}/CyO,GFP ; dpp-Gal4, UAS-GFP^{nls} /TM6B	This paper	N/A
y w; FRT40A ex^{BQ} / CyO,GFP; UAS-Ras^{V12}/ TM6B	This paper	N/A
y w; FRT40A ex^{BQ} / CyO,GFP; UAS-Raf^{GOF} / TM6B	This paper	N/A
y w; FRT40A ex^{AP50} / CyO,GFP; UAS-EGFR^{top} / TM6B	This paper	N/A
y w; UAS-EGFR^{top}	Queenan et al., 1997	N/A
UAS-cic-RNAi / CyO	VDRC http://stockcenter.vdrc.at/control/main	103805
y w, vkg-GFP/CyO,YFP; FRT82B cic^{Q474X} wts^{149}/ TM6B	This paper (*vkg-GFP* was from Bruno Lemaitre, EPFL)	N/A
y w, FRT82B cic^{Q474X} / TM6B	Tseng et al., 2007	N/A
y w, FRT82B ras^{DC408}/ TM6B	Tseng et al., 2007	N/A
y w, FRT82B ras^{DC408} cic^{Q474X} / TM6B	Tseng et al., 2007	N/A
y w, FRT82B wts^{149}/ TM6B	null allele, Georg Halder, KU Leuven	N/A
y w, FRT82B cic^{Q474X} wts^{149}/ TM6B	This paper	N/A
y w eyflp ; FRT82B M(3) ubiGFP^{nls} / TM6B	This paper	N/A
y ubxflp ; FRT82B M(3) ubiGFP^{nls} / TM6B	Georg Halder, KU Leuven	N/A
y w ; FRT 82B	Georg Halder, KU Leuven	N/A
FRT40A ex^{AP50}, UAS-SOCS-36E / CyO,GFP ; UAS-EGFR^{top} / TM6B	This paper	N/A
y w; FRT40A ex^{e1}/CyO,GFP; dpp-Gal4, UAS-GFP, UAS-pnt-RNAi / TM6B	This paper	*UAS-pnt-RNAi* is BL31936
y w ; UAS-cic-RNAi / CyO,YFP,Dfd ; UAS-Yki	This paper	N/A

(Continued on next page)

REAGENT or RESOURCE	SOURCE	IDENTIFIER
y w hsflp ; *FRT40A ex*[e1]/ *CyO,GFP*; *act < CD2 < Gal4, UAS-GFP / TM6B*	Georg Halder, KU Leuven	N/A
y w hsflp ; *FRT82B wts*[P2] *ubiGFP / TM6B*	This paper	N/A
ex[BQ] and *ex*[AP50] are null alleles	Hamaratoglu et al., 2006	N/A
Software and Algorithms		
iRegulon	Janky et al., 2014	http://iregulon.aertslab.org
i-cisTarget	Imrichová et al., 2015	https://gbiomed.kuleuven.be/apps/lcb/i-cisTarget/
Multiple Experiment Viewer 4.8.1	Saeed et al., 2003	https://sourceforge.net/projects/mev-tm4/
DESeq2	Love et al., 2014	https://bioconductor.org/packages/release/bioc/html/DESeq2.html
TopHat2 Bowtie2	Kim et al., 2013	http://bowtie-bio.sourceforge.net/bowtie2/index.shtml
Htseq-count	Anders et al., 2015	http://www-huber.embl.de/HTSeq
NMF package	Gaujoux and Seoighe, 2010	https://cran.r-project.org/web/packages/NMF/index.html

CONTACT FOR REAGENT AND RESOURCE SHARING

Requests for resources and reagents should be directed and will be fulfilled by the Lead Contact, Fisun Hamaratoglu (fisun.hamaratoglu@unil.ch).

EXPERIMENTAL MODEL AND SUBJECT DETAILS

Drosophila melanogaster were grown on standard fly medium and kept in 26°C incubators. The imaginal discs were dissected from larvae of both sexes.

METHOD DETAILS

Immunohistochemistry
The crosses were transferred to fresh tubes every day (for more precise staging practices see (Hamaratoglu et al., 2011)). For immu-nohistochemistry, dissected larval complexes, free of fat body and salivary glands, were fixed in 4% pfa in PBS for 25 minutes. After extensive washes, the discs were blocked in PBTN (PBS+0.03% TritonX+2% Normal Donkey Serum, Fisher Scientific, NC9624464) for 1h. Primary antibody incubation was O/N in the cold room; secondary antibody incubation was for 2h. All incubation and wash steps were done in ice-cold solutions on a rotator at RT with the exception of the primary antibody incubation. After final washes, all excess liquid was removed and 2 drops of Vectashield (Vector Labs, H-1200) were added; the discs were mounted on slides in Vectashield the next day. Antibodies used were: m-β-gal (1:2000, Promega), r-ELAV (1:1500, DSHB-7E8A10), m-Yan (1:10, DSHB-8B12H9), r-Ci (1:150, Robert A. Holmgren), rb-Pnt (1:2000), gp-Cic (1:300, Iswar Hariharan).

Antibody Production
Antibodies against Pnt and Cic were produced by GenScript. They were antigen affinity purified and resuspended in PBS pH 7.4 / 0.02% sodium azide at the following concentrations: anti-rabbit-Pnt = 2.622 mg/ml, anti-rabbit-Cic = 1.715 mg/ml. Pnt C-term half (last 298 aas), that is common to all isoforms, was used as an epitope and the antibody recognizes overexpressed Pnt-P1 and Pnt-P2. For Cic, a C-term small peptide (NDSDMDDTPFDYRK) was used to generate a peptide antibody.

RNA-seq Sample Preparation and Sequencing
Wing discs were collected from 12-35 larvae under sterile conditions and immediately lysed. Genotypes used were: wt, day 5 (y w ubxflp/ y w; FRT82B M(3) ubiGFP/ FRT 82B), *cic*, day 5 (y w ubxflp/ y w; FRT82B M(3) ubiGFP/ FRT 82B *cic*[Q474X]), *wts*, day 5 and day 9 (y w ubxflp/ y w; FRT82B M(3) ubiGFP/ FRT 82B *wts*[149]), *cic wts*, day 5 and day 9 (y w ubxflp/ y w; FRT82B M(3) ubiGFP/ FRT 82B *cic*[Q474X] *wts*[149]). RNA extraction was done using Ambion RNAqueous Micro kit. 500ng total RNA and Illumina TruSeq mRNA Library Prep reagents were used according to the protocol recommended by the manufacturer for library preparation and the sequencing was done using Illumina HiSeq2500.

Isolation of Chromatin from Imaginal Discs

We used larvae of following genotypes: wild-type control (y w ubxflp/ y w; FRT82B M(3) ubiGFP/ FRT 82B), 500 wing discs/ sample; *wts* mutant discs from day9 giant larvae (y w ubxflp/ y w; FRT82B M(3) ubiGFP/ FRT 82B *wts*[149]), 100 wing discs/ sample; *cic wts* mutant discs from day9 giant larvae (y w ubxflp/ y w; FRT82B M(3) ubiGFP/ FRT 82B *cic*[Q474X] *wts*[149]) , 100 wing discs/ sample.

Third instar larvae were dissected in cold PBS and imaginal disc complexes (anterior one third of the larvae after removing the fat body and salivary glands) were fixed in 1 ml fixation buffer (50 mM 4-(2-hydroxyethyl)-1-piperazineethanesulfonic acid [HEPES], pH 7.5; 1 mM ethylenediaminetetraacetic acid [EDTA]; 0.5 mM ethylene glycol tetraacetic acid [EGTA]; 100 mM NaCl; 2% formaldehyde) for 30 min at room temperature. Fixed disc complexes were washed 3x fast and 2x 20 minutes with PBST (PBS, pH 7.4; 0.1% Triton X-100; 0.1% Tween-20), and were stored at 4°C until enough discs were obtained. 100-500 wing discs were dissected away from the cuticle and resuspended in buffer A2 (15 mM HEPES, pH 7.5; 140 mM NaCl; 1 mM EDTA; 0.5 mM EGTA; 1% Triton X-100; 0.1% sodium deoxycholate; 0.1 % sodium dodecyl sulfate [SDS]; 0.5 % *N*-lauroylsarcosine; 1× Roche complete protease inhibitor cocktail, cat. no. 5056489001). Tubes were flash frozen in liquid nitrogen and stored at -80°C. Imaginal discs were pooled to reach 500 wt discs (or 100 mutant), and sonication was performed in a Bioruptor sonicator for 5 min (30 s on/off cycle at the "high" setting) in buffer A2. Following centrifugation (16,000 × g; 10 min at 4°C), the supernatant containing soluble chromatin was transferred to fresh tubes, and used for ChIP-nexus.

ChIP-nexus

20 μg antibody (rb-Sd (Ikmi et al., 2014) or rb-Cic) was incubated with Protein A and Protein G beads for 6 hours. Chromatin isolated from 500 wild-type or 100 mutant imaginal discs were added to antibody coated beads and incubated overnight at 4°C with end to end rotation in a 1ml volume. ChIP-nexus digestion and library preparation was performed as published (He et al., 2015), with minor modifications. To repair the DNA ends, NEBNext End Repair Module (NEB#E6050) was used, and reactions were set up in a 50 μl volume at 20°C for 1 h with gentle mixing in a thermomixer. The dA tailing reactions were set up in a 50 μl final volume, incubated for 30 min at 37°C using the NEBNext dA-Tailing Module(NEB#E6053). The ChIP-nexus adaptors were then ligated by incubation at 25°C for 60 min in 200 U/μl Quick T4 DNA ligase (New England BioLabs, M2200) and 60 nmol/μl Nex_adaptor in 50 μl 1× Quick Ligation Reaction Buffer (New England BioLabs, B6058S). To fill the ends of the adaptors, each sample was incubated at 37°C for 30 min with 0.1 U/μl Klenow fragment (3′→5′ exo⁻) (New England BioLabs, M0212) and 0.1 mmol/μl dNTPs in 50 μl 1× NEBuffer 2. The ends were then trimmed by incubation at 12°C for 5 min in 0.09 U/μl T4 DNA polymerase (New England BioLabs, M0203) and 0.1 mmol/μl dNTPs in 50 μl 1× NEBuffer 2. For λ-exonuclease digestion, each sample was incubated at 37°C for 60 min with constant agitation in 0.2 U/μl λ-exonuclease (New England BioLabs, M0262), 5% dimethyl sulfoxide (DMSO) and 0.1% Triton X-100 in 100 μl 1× Lambda Exonuclease Reaction Buffer (New England BioLabs, B0262S). Finally, RecJf exonuclease digestion was carried out at 37°C for 60 min with constant agitation in 0.75 U/μl RecJf exonuclease (New England BioLabs, M0264), 5% DMSO and 0.1% Triton X-100 in 100 μl 1× NEBuffer 2. After each enzymatic treatment, the chromatin was washed with the following buffers: wash buffer A (10 mM Tris-EDTA, 0.1% Triton X-100), wash buffer B (150 mM NaCl, 20 mM Tris-HCl, pH 8.0, 5 mM EDTA, 5.2% sucrose, 1.0% Triton X-100, 0.2% SDS), wash buffer C (250 mM NaCl, 5 mM Tris-HCl, pH 8.0, 25 mM HEPES, 0.5% Triton X-100, 0.05% sodium deoxycholate, 0.5 mM EDTA), wash buffer D (250 mM LiCl, 0.5% IGEPAL CA-630, 10 mM Tris-HCl, pH 8.0, 0.5% sodium deoxycholate, 10 mM EDTA) and Tris buffer (10 mM Tris, pH 7.5, 10 mM Tris, pH 8.0, or 10 mM Tris, pH 9.5, depending on the next enzymatic step). Residual buffer was drained before the next enzymatic reaction was initiated. After RecJf digestion, the Dynabeads were washed three times with RIPA buffer (50 mM HEPES, pH 7.5, 1 mM EDTA, 0.7% sodium deoxycholate, 1% IGEPAL CA-630, 0.5 M LiCl). The DNA was eluted, reverse crosslinked and subject to ethanol precipitation. Each sample was resuspended in 11.25 μl H₂O, 1.5 μl 10× CircLigase buffer, 0.75 μl 1 mM ATP, 0.75 μl 50 mM MnCl₂, 0.75 μl CircLigase (Epicentre) and incubated at 60°C for 60 min for self-circularization. To anneal the oligonucleotide complementary to the BamHI restriction site, 26 μl H₂O, 5 μl FastDigest buffer (Fermentas) and 1 μl 10 μM cut oligo was added to each sample. The mixture was incubated on a thermocycler as follows: 95°C for 5 min, then ramped down to 25°C at a rate of ∼3.5°C/min and held at 25°C for 30 min. For BamHI digestion, 3 μl Fastdigest BamHI was added, and the sample was incubated at 37°C for 30 min. The samples were then precipitated by the addition of 150 μl TE buffer, 30 μg glycogen, 20 μl 3 M/l sodium acetate (pH 5.5) and 500 μl 100% ethanol and incubated at −80°C for 2.5 h. After centrifugation at 4°C for 30 min at 16,100*g*, the samples were washed with 500 μl 80% ethanol, dried overnight at room temperature and resuspended in H₂O. PCR amplification was performed using the NEBNext High-Fidelity 2X PCR Master Mix (NEB#M0541). 1 μl each of 10 μM universal and barcoded PCR primers were used for each reaction and DNA was amplified for 18 cycles. The ChIP-nexus libraries were gel purified before submitting for sequencing and were sequenced with Illumina NextSeq 500.

QUANTIFICATION AND STATISTICAL ANALYSIS

iRegulon Normalized Enrichment Scores (NES)

For a certain gene set as input, the enrichment for each motif (9713 unique PWMs) is determined by the Area Under the Recovery Curve (AUC) of the cumulative recovery curve, along the whole-genome ranking. A Normalized Enrichment Score (NES) is computed as the AUC value of the motif minus the mean of all AUCs for all motifs and divided by the standard deviation of all AUCs. This is very

similar to a z-score, and a NES score of 3 corresponds to an FDR (false discovery rate) of 0.03 to 0.09. A high NES for a certain motif indicates that this motif is significantly overrepresented in the immediate regulatory space (5kb upstream and all introns) of the genes from the input set (Janky et al., 2014).

RNA-seq Analysis

Raw reads were cleaned for adapter sequences using *fastq-mcf.* Cleaned reads were mapped on *Drosophila melanogaster* FlyBase release r6.03 using TopHat2 (Kim et al., 2013) (Bowtie2/2.2.1-intel-2014a). Htseq-count (Anders et al., 2015) (HTSeq/0.6.1p1-foss-2014a-Python-2.7.6) was used to assign reads to genes using the dmel-all-r6.03.gff template. The raw counts matrix (6 conditions each with 3 biological replicates) was further processed and size factor was normalized in R. The list of 350 upregulated genes in *cic wts* double mutants vs wild type controls was obtained using DESeq2 (Love et al., 2014) (differential analysis with 3 replicates, cutoff; average expression > 50, logFC > 0.5 and adjusted P-value < 0.01). These 350 genes were subdivided into four groups, based on their normalized expression values ($\log_2$ transformed) in the day_5 samples, using an unsupervised clustering method (Self Organizing Tree Algorithm, standard parameters in MeV) (Saeed et al., 2003). Genes from *wts* cluster whose expression increased more than 1.3 folds from *wts* to *cic wts* were added to the synergetic cluster. The final set of 46 synergistic genes was obtained by filtering out genes whose expression dropped below wild type levels in *cic wts* day_9. Motif enrichment analysis was carried out on each gene set using iRegulon v1.4 (Janky et al., 2014), (plugin for Cytoscape) using a library of 9713 PWMs, taking the full transcript and 5kb upstream of each gene into account. Expression heat-maps were generated with the NMF package in R (Gaujoux and Seoighe, 2010), using $\log_2$ normalized counts and these options: scale="row", Rowv=F ,Colv=NA, annRow=medianexp.

ChIP-nexus Analysis

Mapped bam files and bigwig files were generated as described from the sequenced reads (He et al., 2015). Scalloped peaks were called on the (unclipped) mapped reads, using the MACS2 software suite (Feng et al., 2011) (macs2 callpeak -t sd_genotype.bam -g dm -n sd_genotype.macs2 –keep-dup all –call-summits). ChIP peaks with sufficient reads (fold change > 10) were retained for further analysis. Cic peaks were called on the (unclipped) mapped reads, using Cic-ChIP in *cic wts* mutants samples as control (macs2 callpeak -t cic_genotype.bam -g dm -n cic_genotype.macs2 –bdg –nomodel -c cic_cic.wts.bam). Using the negative controls (Cic pulldown in *cic wts* discs) removed most of the noise, allowing us to use all the called peaks for further analysis. The retained ChIP peaks were used as input sets for i-cisTarget (Imrichová et al., 2015), a tool that identifies significantly enriched motifs in a set of (ChIP) regions. Directly bound regions were defined as those regions that had their respective transcription factor DNA binding motifs significantly enriched.

DATA AND SOFTWARE AVAILABILITY

RNA-seq and ChIP-nexus datasets have been deposited to NCBI's Gene Expression Omnibus. They are accessible through the accession number GEO: GSE96868.